Electronic Supplementary Material (ESI) for Dalton Transactions.

Supporting Information

Macrocyclic NHC complexes of group 10 elements with enlarged aromaticity for biological studies

Marco A. Bernd,[a],† Elisabeth B. Bauer,[a],† Jens Oberkofler,[a] Andreas Bauer,[b] Robert M. Reich[a] and Fritz E. Kühn*[a]

Table of contents:

[a] Department of Chemistry and Catalysis Research Center, Molecular Catalysis, Technische Universität München, Lichtenbergstr. 4, 85747 Garching bei München, Germany
E-mail: fritz.kuehn@ch.tum.de
[b] Department of Chemistry and Catalysis Research Center, Chair of Organic Chemistry I, Technische Universität München, Lichtenbergstr. 4, 85747 Garching bei München, Germany
E-mail: andreas.bauer@tum.de
† These authors contributed equally.

NMR spectra

Calix[4]imidazoyl-nickel(II) Hexafluorophosphate (A)

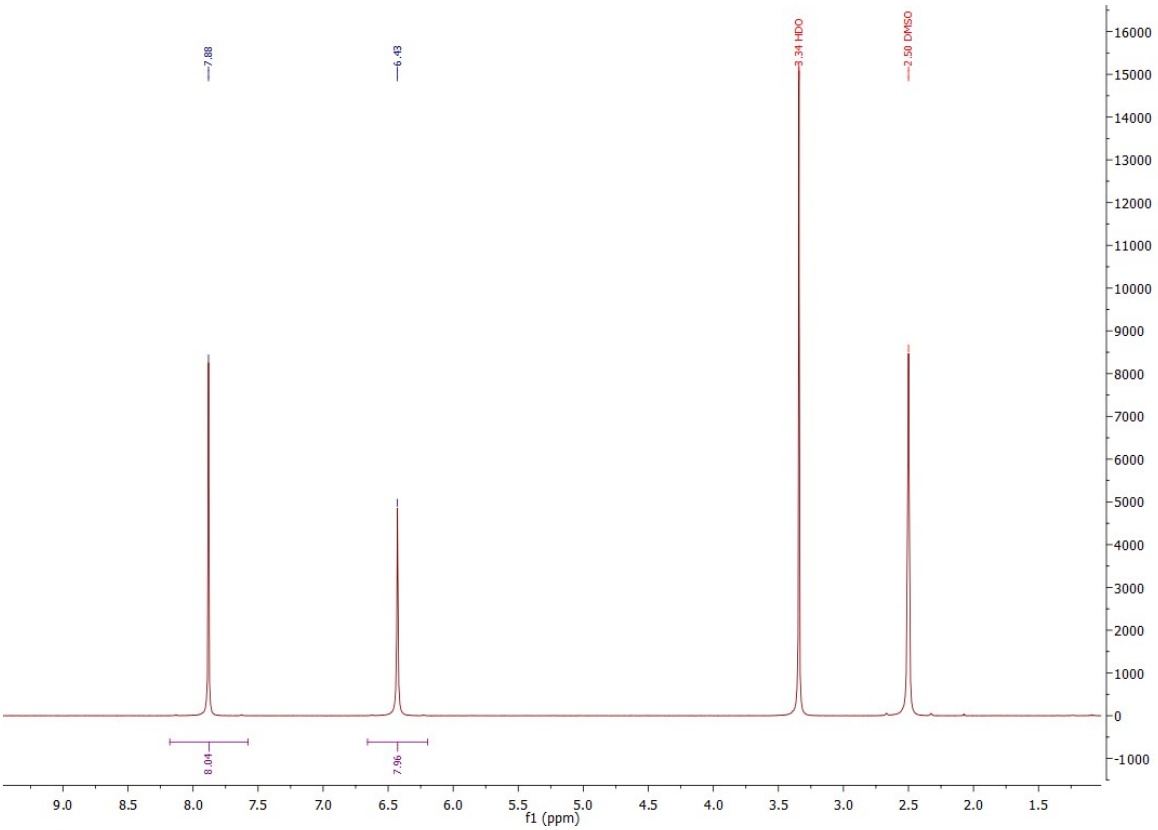

Figure 1: ^{1}H-NMR spectrum of calix[4]-imidazoyl-nickel(II) hexafluorophosphate (**A**) in DMSO-d_6.

Calix[4]imidazoyl-palladium(II) Hexafluorophosphate (B)

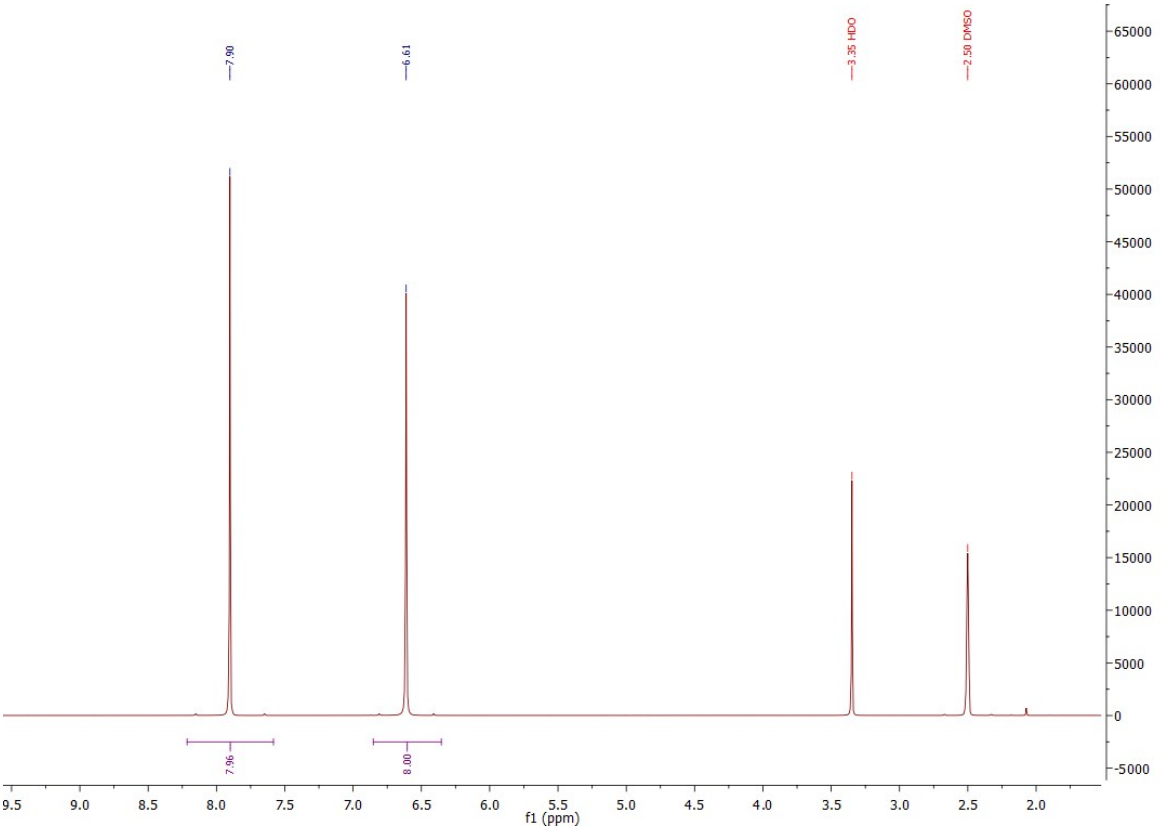

Figure 2: ^{1}H-NMR spectrum of calix[4]-imidazoyl-palladium(II) hexafluorophosphate (**B**) in DMSO-d_6.

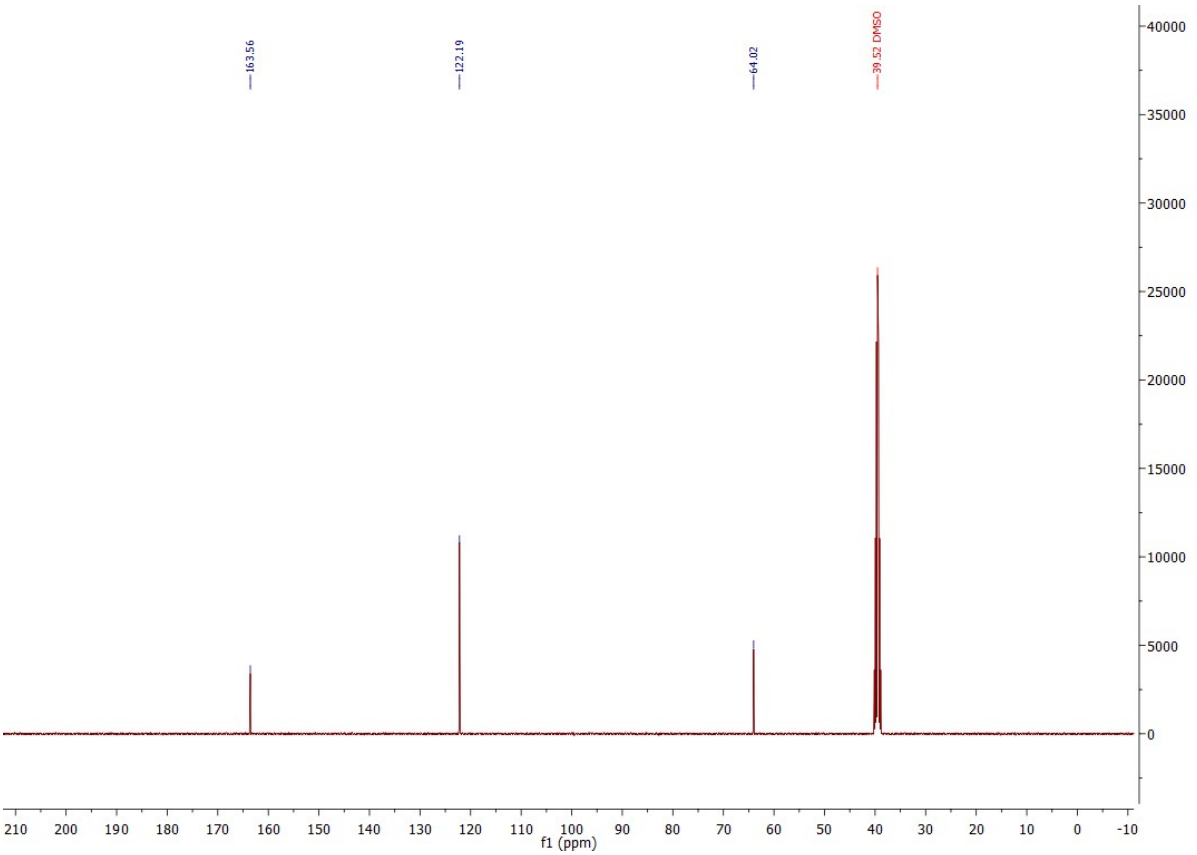

Figure 3: ^{13}C-NMR spectrum of calix[4]-imidazoyl-palladium(II) hexafluorophosphate (**B**) in DMSO-d_6.

Calix[4]imidazoyl-platinum(II) Hexafluorophosphate (C)

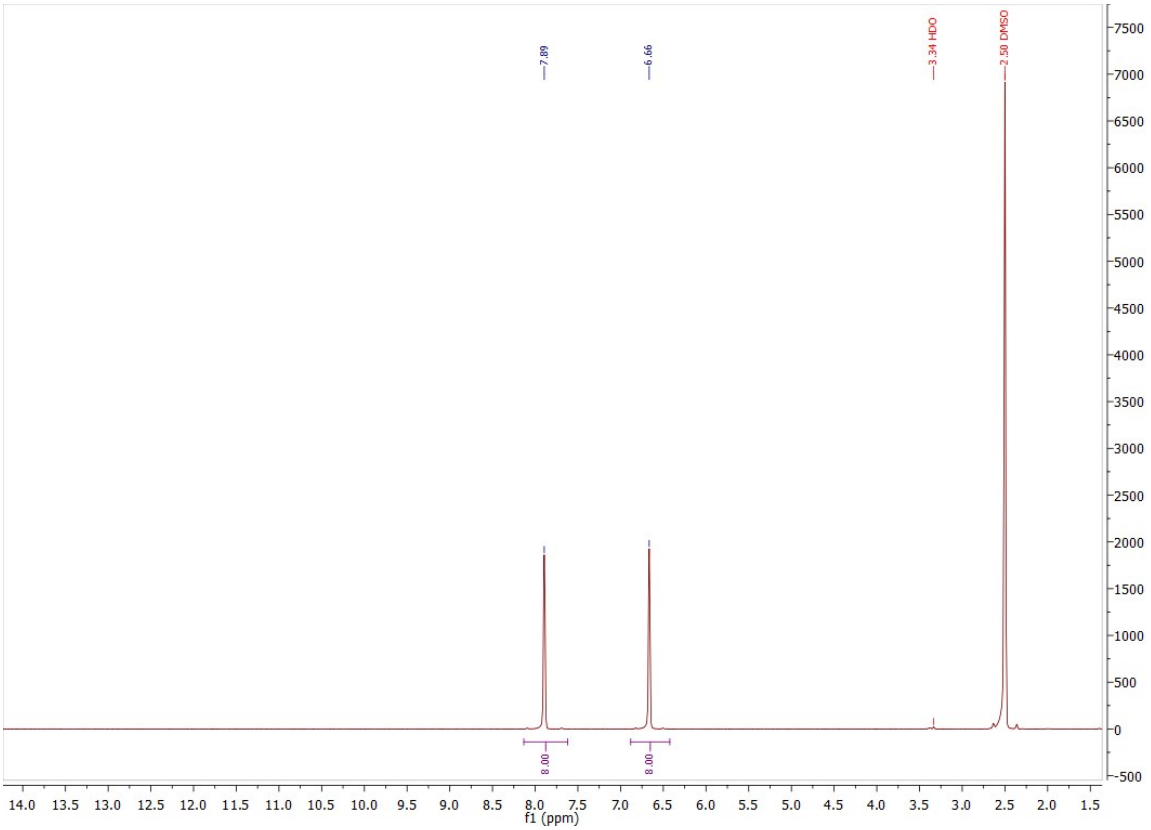

Figure 4: ^{1}H-NMR spectrum of calix[4]-imidazoyl-platinum(II) hexafluorophosphate (**C**) in DMSO-d_6.

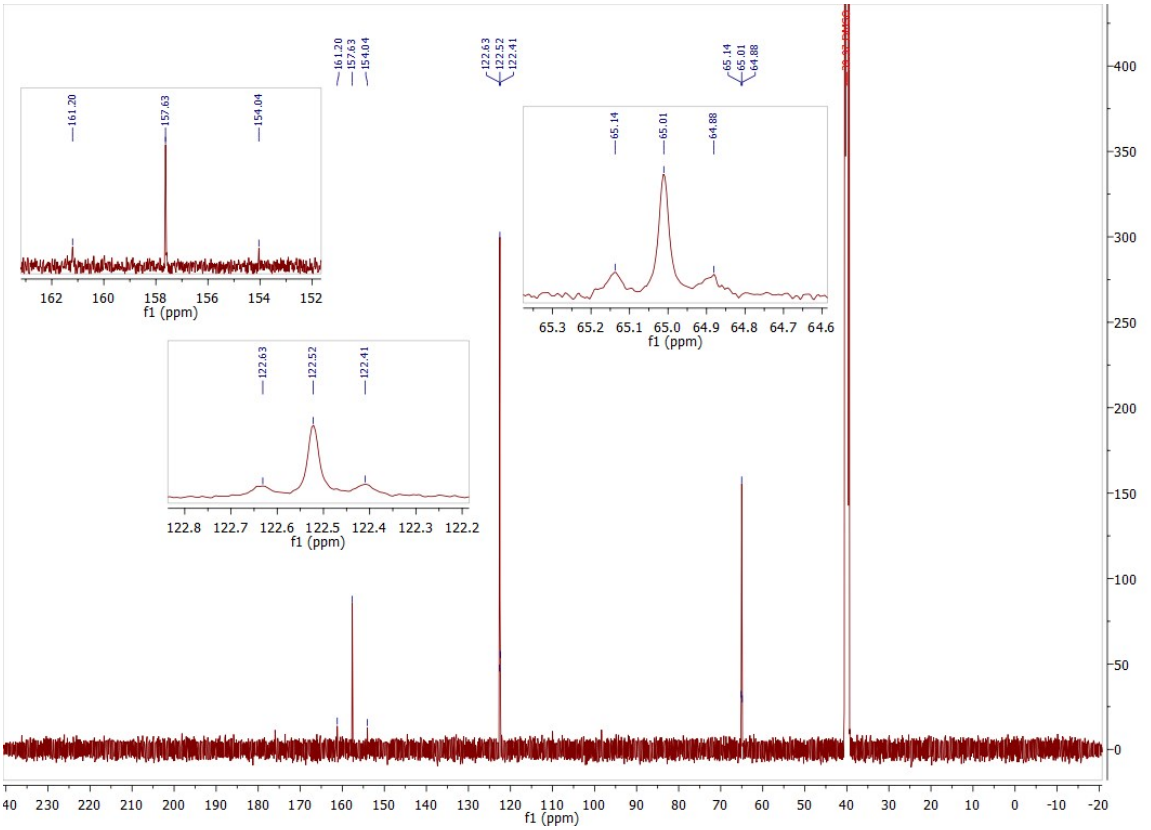

Figure 5: ^{13}C-NMR spectrum of calix[4]-imidazoyl-platinum(II) hexafluorophosphate (**C**) in DMSO-d_6. Coupling of ^{195}Pt with respective ^{13}C is visible as satellite duplets.

Calix[4]-benzimidazoyl-nickel(II) Trifluoromethanesulfonate (**D**)

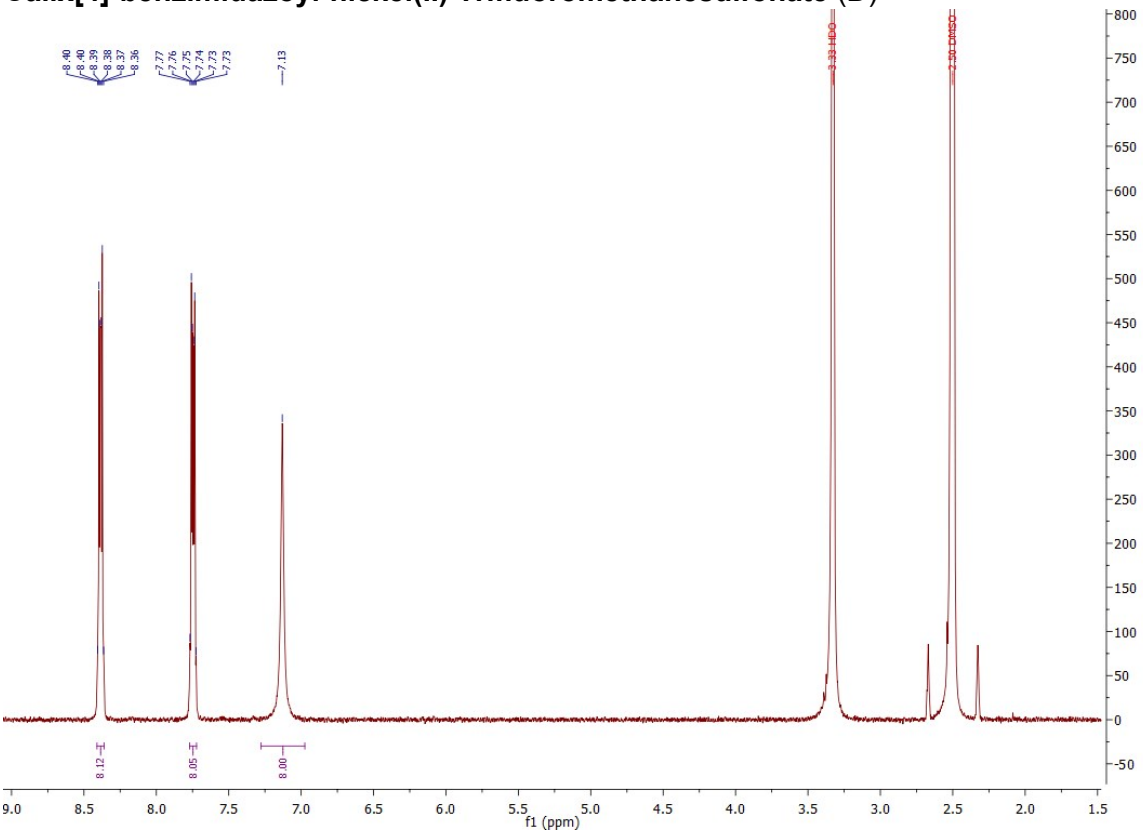

Figure 6: ^{1}H-NMR spectrum of calix[4]-benzimidazoyl-nickel(II) trifluoromethanesulfonate (**D**) in DMSO-d_6.

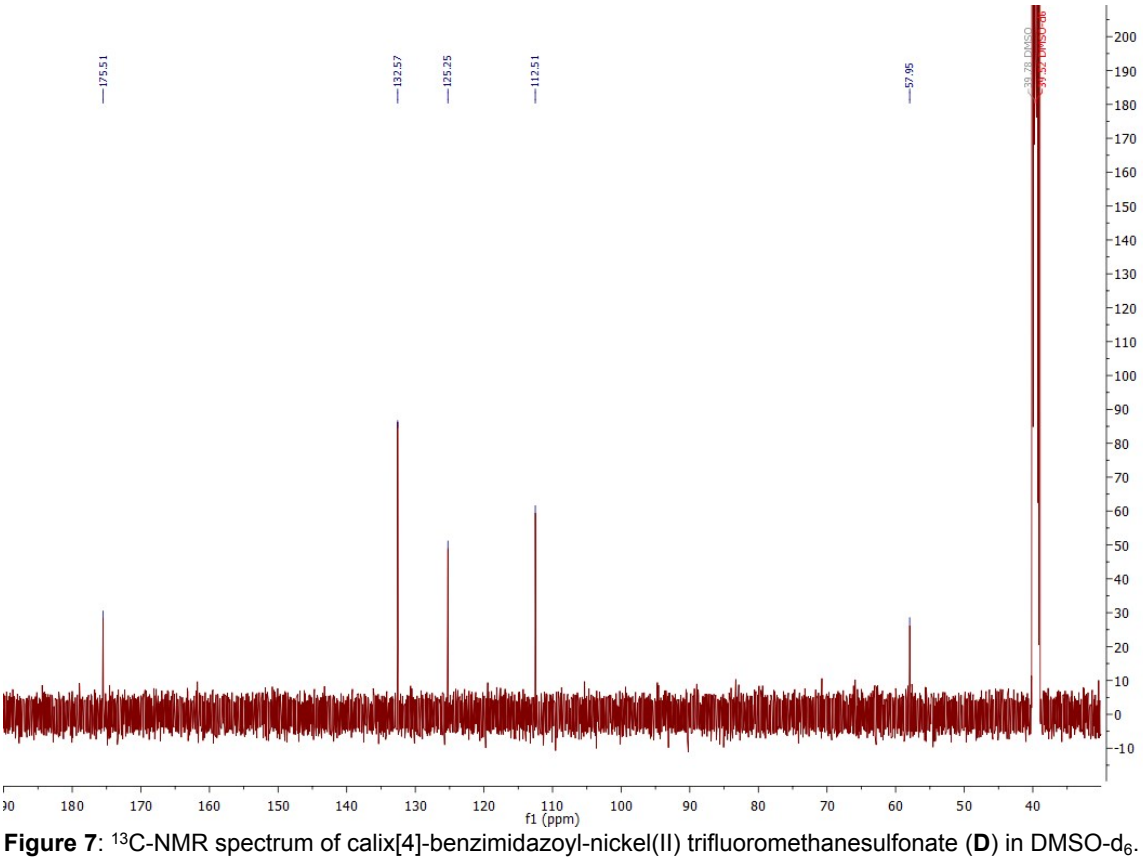

Figure 7: ^{13}C-NMR spectrum of calix[4]-benzimidazoyl-nickel(II) trifluoromethanesulfonate (**D**) in DMSO-d_6.

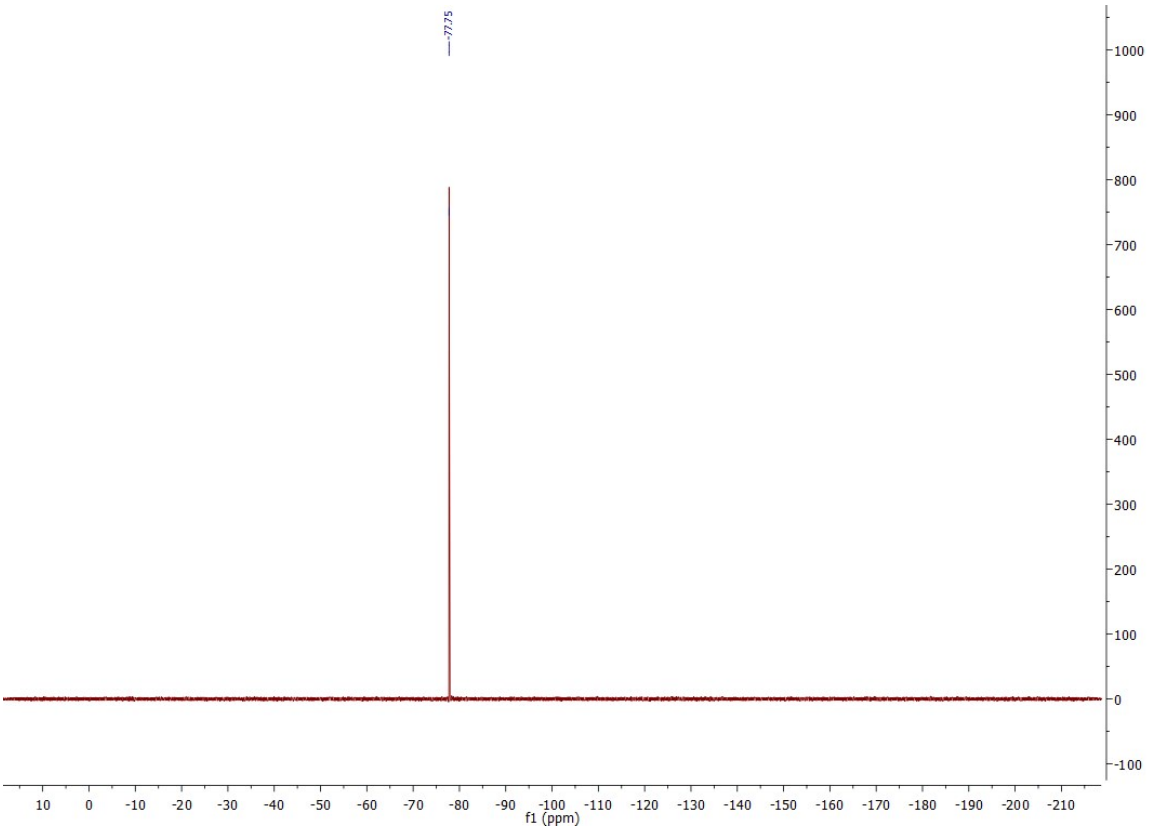

Figure 8: ^{19}F-NMR spectrum of calix[4]-benzimidazoyl-nickel(II) trifluoromethanesulfonate (**D**) in DMSO-d_6. No reference standard was added, due to only the anion signal being of interest.

Calix[4]-benzimidazoyl-palladium(II) Trifluoromethanesulfonate (**E**)

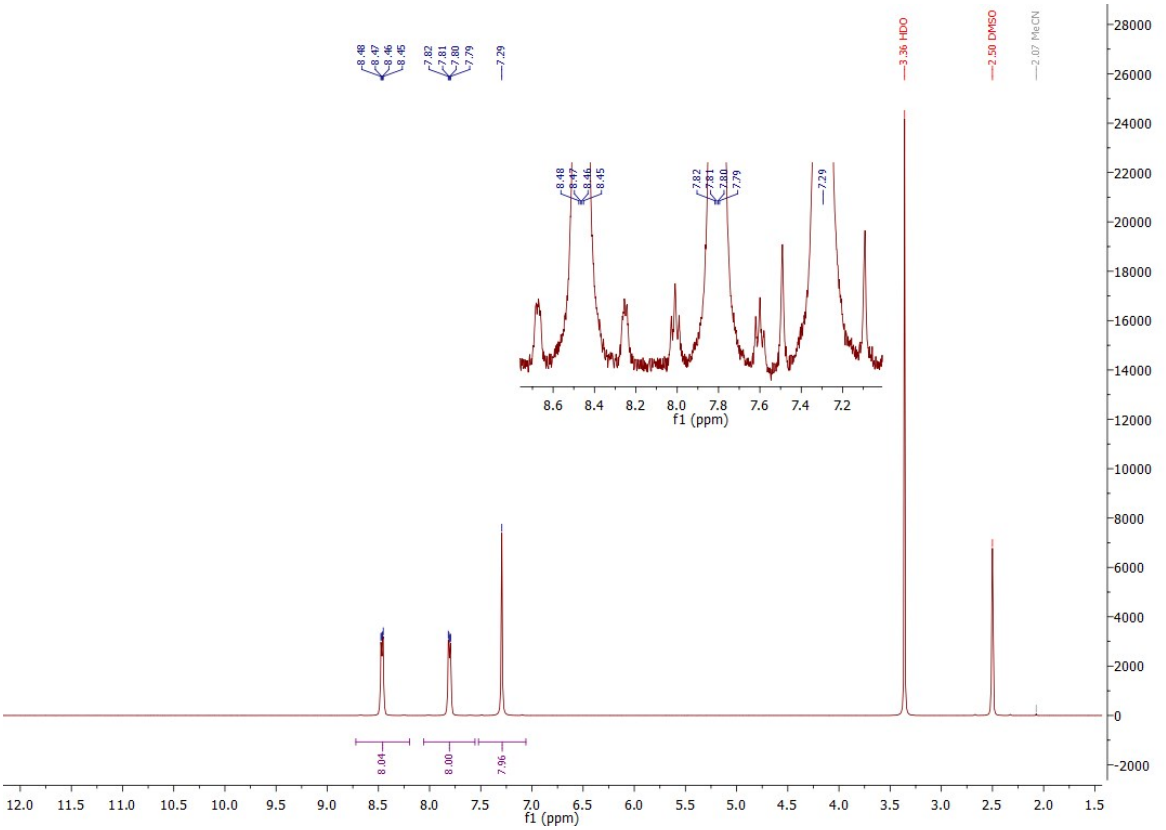

Figure 9: ^{1}H-NMR spectrum of calix[4]-benzimidazoyl-palladium(II) trifluoromethanesulfonate (**E**) in DMSO-d_6.

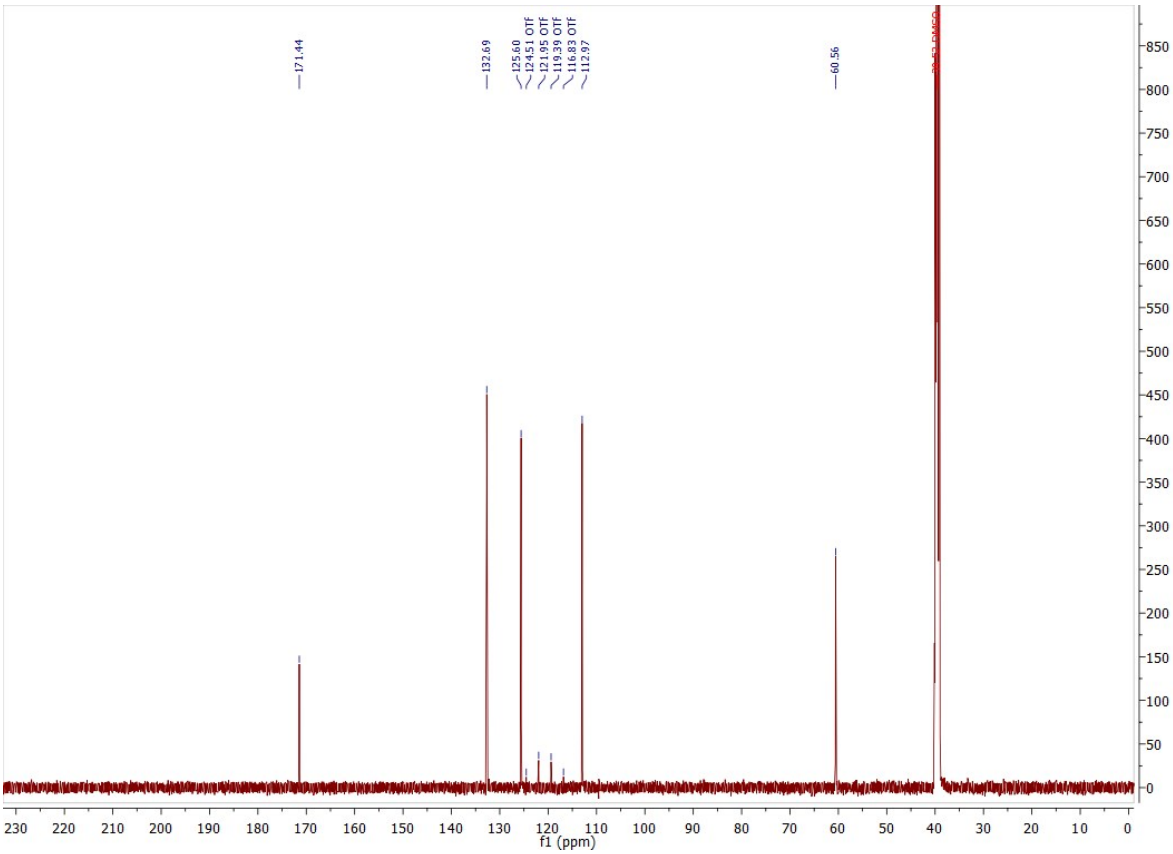

Figure 10: ^{13}C-NMR spectrum of calix[4]-benzimidazoyl-palladium(II) trifluoromethanesulfonate (**E**) in DMSO-d_6.

Calix[4]-benzimidazoyl-platinum(II) Trifluoromethanesulfonate (F)

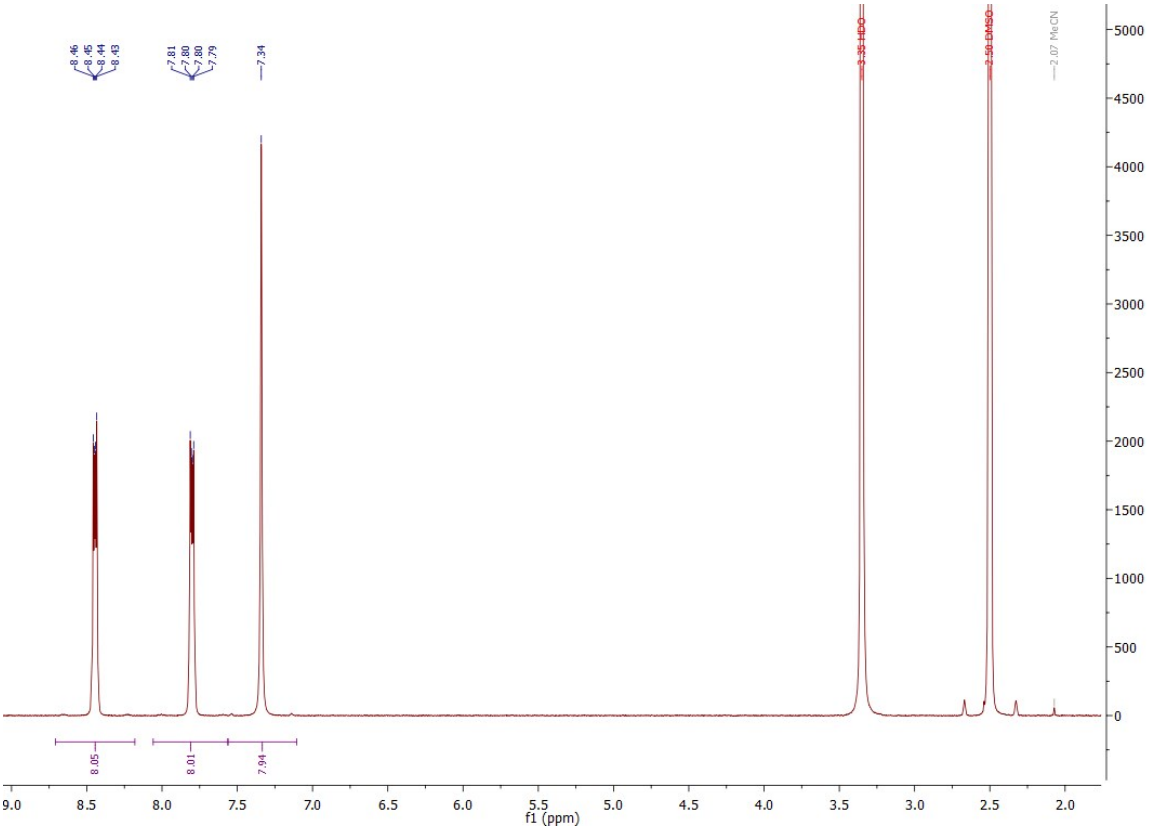

Figure 11: ^{1}H-NMR spectrum of calix[4]-benzimidazoyl-platinum(II) trifluoromethanesulfonate (**F**) in DMSO-d_6.

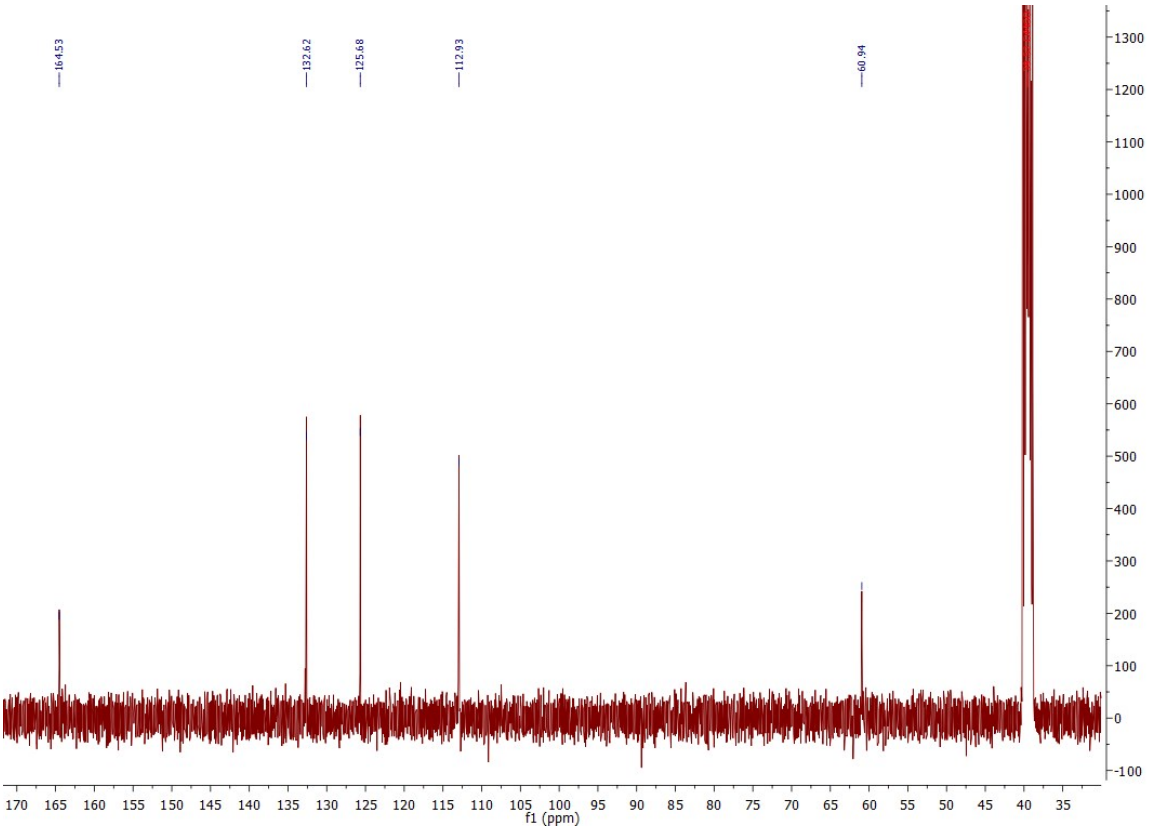

Figure 12: ^{13}C-NMR spectrum of calix[4]-benzimidazoyl-platinum(II) trifluoromethanesulfonate (**F**) in DMSO-d_6.

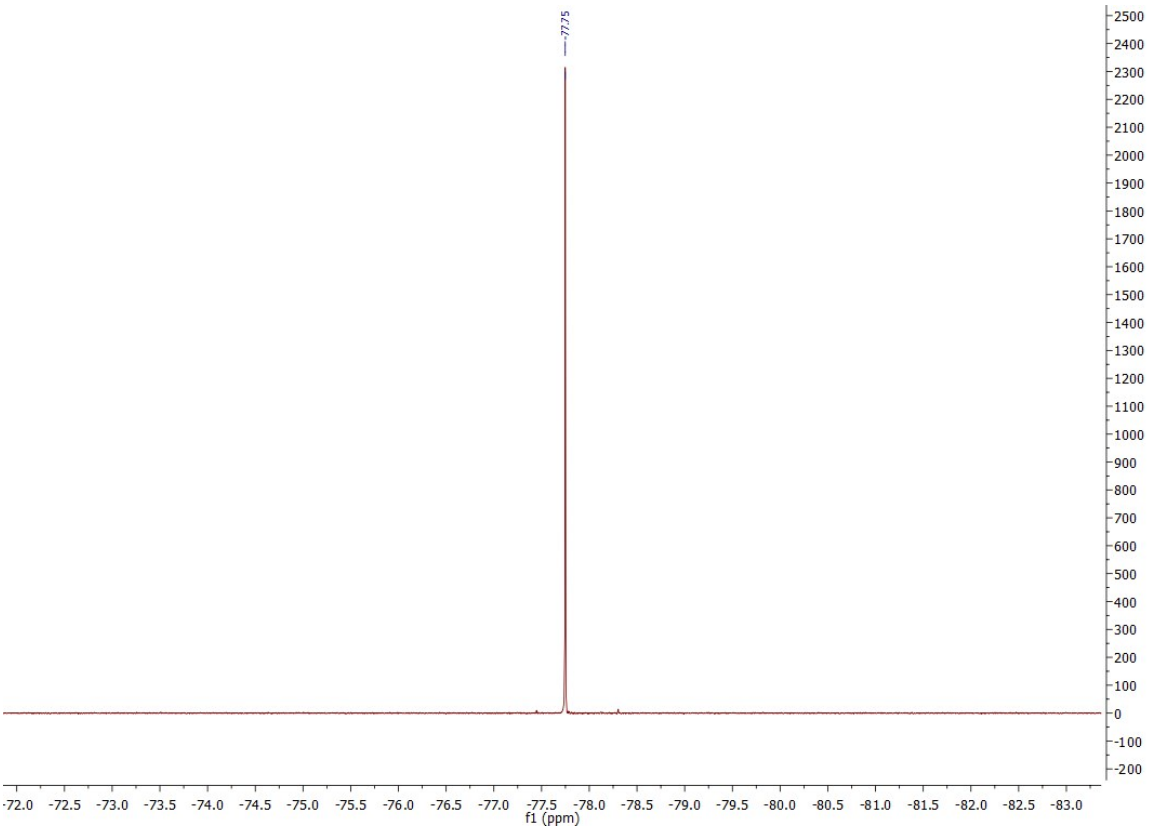

Figure 13: ^{19}F-NMR spectrum of calix[4]-benzimidazoyl-platinum(II) trifluoromethanesulfonate (**F**) in DMSO-d_6. No reference standard was added, due to only the anion signal being of interest.

Single Crystal X-Ray Diffraction

Table 1: Crystallographic data of compounds **D** – **F.**

Compound	**D**	**E**	**F**
formula	$C_{34}H_{30}AgCl_3N_8NiOS$	$C_{36}H_{30}F_6N_8O_7PdS_3$	$C_{34}H_{24}F_6N_8O_6PtS_2$
CCDC number	2014590	2014591	2014592
fw	871.65	1003.26	1013.81
color/habit	clear yellow block	clear blue fragment	clear colourless plate
Cryst. Dimens. [mm^3]	0.044 x 0.073 x 0.210	0.035 x 0.122 x 0.266	0.224 x 0.283 x 0.310
Cryst. Syst.	orthorhombic	monoclinic	Triclinic
space group	P 2_1/n 2_1/m 2_1/a	P 1 2/c 1	P -1
a [Å]	28.136(2)	16.755(16)	11.3026(9)
b [Å]	17.1992(13)	14.457(16)	11.4231(8)
c [Å]	7.4871(6)	17.367(17)	16.8559(11)
α [deg]	90	90	107.288(3)
β [deg]	90	116.67(2)	109.258(3)
γ [deg]	90	90	93.248(3)
V [$Å^3$]	3623.1(5)	3759.(10)	1928.5(2)
Z	4	4	2
T [K]	100(2)	100(2)	100(2)
D_{calcd} [g/cm^{-3}]	1.598	1.769	1.880
μ [mm^{-1}]	1.379	0.752	3.891
F(000)	1760	2024	1076
ϑ range [deg]	2.78 to 27.48	1.92 to 25.35	2.46 to 25.03
index range (h, k, l)	–36 ≤ h ≤ +36 –22 ≤ k ≤ +22 –9 ≤ l ≤ +9	-20 ≤ h ≤ +20 -17 ≤ k ≤ +17 -19 ≤ l ≤ +20	-13 ≤ h ≤ +13 -13 ≤ k ≤ +13 -20 ≤ l ≤ +19
Reflections collected	170003	114167	67689
no. of indep refIns/R_{int}	4295/0.0600	6898/0.0661	6752/0.0619
no. of data/ restraints/params	4295/15/233	6898/108/591	6752/246/626
R1/wR2 (*I*>2σ(I))	0.0382/0.0804	0.0378/0.0830	0.0458/0.1086
R1/wR2 (*all data*)	0.0449/0.0831	0.0446/0.0858	0.0486/0.1097
GOF (on F^2)	1.086	1.139	1.193
Largest diff peak and hole [e $Å^{-3}$]	1.305/-1.852	0.669/-0.658	3.031/-4.243

X-ray Crystallographic Details

Data were collected on a single crystal x-ray diffractometer equipped with a CCD detector (APEX II, κ-CCD), a rotating anode FR591 and a Montel mirror optic using the APEX2 software package (**D**) or a single crystal x-ray diffractometer equipped with a CMOS detector (Bruker APEX III, κ-CMOS), an IMS microsource with MoK_α radiation (λ = 0.71073 Å) and a Helios optic using the APEX3 software package (**E**, **F**).[1] Measurements were performed on single crystals coated with perfluorinated ether. The crystals were fixed on top of a kapton micro sampler and frozen under a stream of cold nitrogen. A matrix scan was used to determine the initial lattice parameters. Reflections were corrected for Lorentz and polarisation effects, scan speed, and background using SAINT.[2] Absorption correction, including odd and even ordered spherical harmonics was performed using SADABS.[3] Space group assignment was based upon systematic absences, E statistics, and successful refinement of the structure. The structures were solved using SHELXS or SHELXT with the aid of successive difference Fourier maps and were refined against all data using SHELXL in conjunction with SHELXLE.[4,5,6] Hydrogen atoms were calculated in ideal positions as follows: Methyl hydrogen atoms were refined as part of rigid rotating groups, with a C–H distance of 0.98 Å and $U_{iso(H)} = 1.5 \cdot U_{eq(C)}$. Other H atoms were placed in calculated positions and refined using a riding model, with methylene and aromatic C–H distances of 0.99 Å and 0.95 Å, respectively, and other C–H distances of 1.00 Å, all with $U_{iso(H)} = 1.2\, U_{eq(C)}$. Non-hydrogen atoms were refined with anisotropic displacement parameters. Full-matrix least-squares refinements were carried out by minimizing $\Sigma w(F_o^2 - F_c^2)^2$ with the SHELXL weighting scheme.[4] Neutral atom scattering factors for all atoms and anomalous dispersion corrections for the non-hydrogen atoms were taken from *International Tables for Crystallography*.[7] A split layer refinement was used for disordered groups and additional SIMU, DELU, RIGU, ISOR and SAME restraints were used, if necessary. Images of the crystal structures were generated with Mercury[8] and PLATON[9]. CCDC (**D**: 2014590; **E**: 2014591; **F**: 2014592) contains the supplementary crystallographic data for this paper. Crystallographic data are provided free of charge by The Cambridge Crystallographic Data Centre.

1. *APEX suite of crystallographic software*, APEX 3, Version 2015-5.2, Bruker AXS Inc., Madison, Wisconsin, USA, 2014/2015.
2. *SAINT,* Versions 8.32B, 8.34A and 8.38A, Bruker AXS Inc., Madison, Wisconsin, USA, 2012/2014/2017.
3. *SADABS,* Versions 2012/1, 2014/5 and 2016/2 Bruker AXS Inc., Madison, Wisconsin, USA, 2012/2014/2016.
4. G. Sheldrick, *Acta Crystallogr.,Sect. A*, 2015, **71**, 3-8.
5. G. Sheldrick, *Acta Crystallogr.,Sect. C*, 2015, **71**, 3-8.
6. C. B. Hübschle, G. M. Sheldrick and B. Dittrich, *J. Appl. Crystallogr.*, 2011, **44**, 1281-1284.
7. *International Tables for Crystallography,* Vol. C (Ed.: A. J. Wilson), Kluwer Academic Publishers, Dordrecht, The Netherlands, 1992, Tables 6.1.1.4 (pp. 500–502), 4.2.6.8 (pp. 219–222), and 4.2.4.2 (pp. 193–199).
8. C. F. Macrae, I. J. Bruno, J. A. Chisholm, P. R. Edgington, P. McCabe, E. Pidcock, L. Rodriguez-Monge, R. Taylor, J. van de Streek and P. A. Wood, *J. Appl. Crystallogr.*, 2008, **41**, 466-470
9. A. Spek, *Acta Crystallogr.,Sect. D*, 2009, **65**, 148-155.

UV/Vis spectroscopy

UV/Vis spectra were collected to identify regions of light absorption, required for luminescence studies. UV/Vis spectra were recorded on an Agilent Cary 60 UV-VIS spectrometer under atmospheric conditions from 25 µM samples in acetonitrile (HPLC gradient grade), using a Hellma cell made of quartz SUPRASIL® with a pathway of 10 mm.

Calix[4]benzimidazolium trifluoromethansulfonate (**L2**)

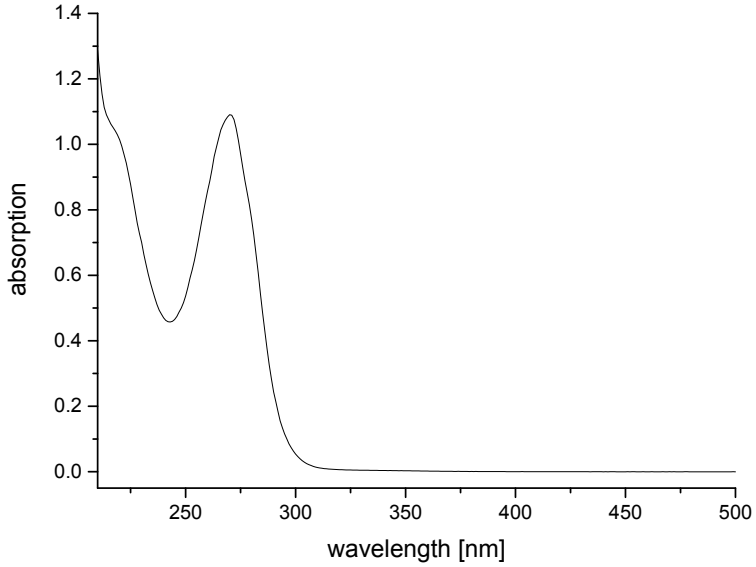

Figure 14: UV/Vis spectrum of calix[4]benzimidazolium trifluoromethansulfonate (**L2**) in acetonitrile at 0.25 µM and a spectral range of 210 – 500 nm. The local maximum is 270.0 nm.

Calix[4]-benzimidazoyl]nickel(II) trifluoromethanesulfonate (**D**)

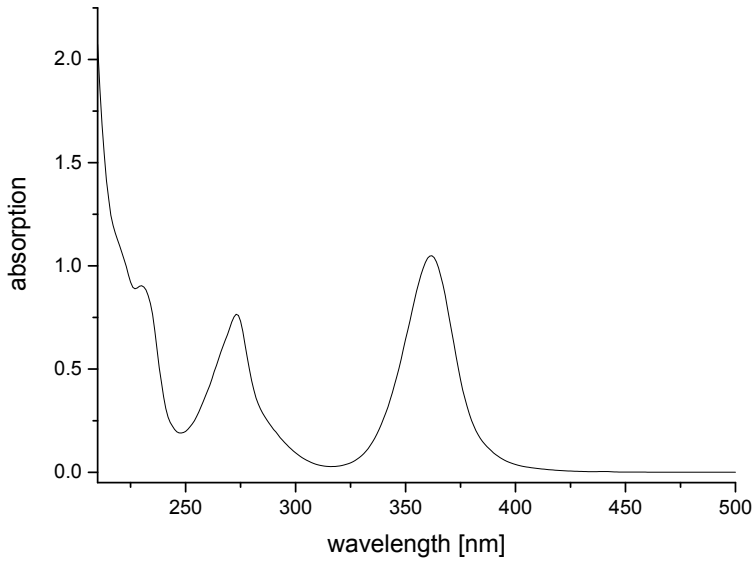

Figure 15: UV/Vis spectrum of calix[4]-benzimidazoyl]nickel(II) trifluoromethanesulfonate (**D**) in acetonitrile at 0.25 µM and a spectral range of 210 – 500 nm. The local maxima are at 230 nm, 273 nm and 362 nm.

Calix[4]-benzimidazoyl]palladium(II) trifluoromethanesulfonate (**E**)

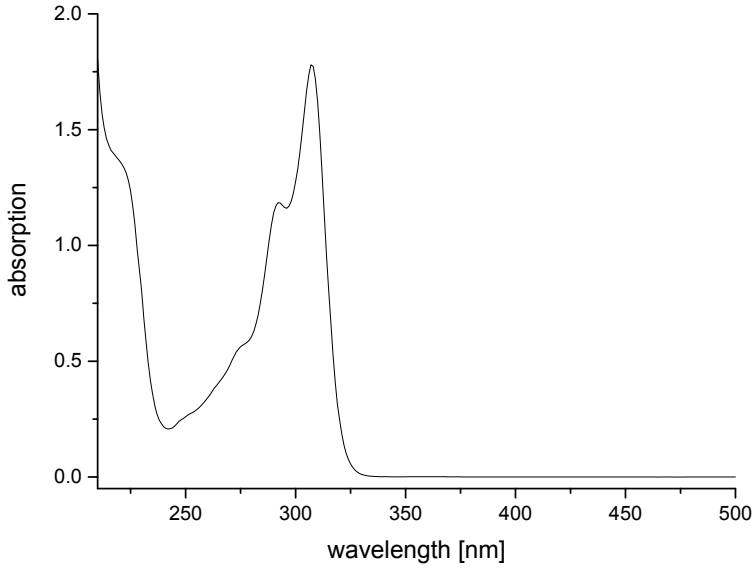

Figure 16: UV/Vis spectrum of calix[4]-benzimidazoyl]palladium(II) trifluoromethanesulfonate (**E**) in acetonitrile at 0.25 μM and a spectral range of 210 – 500 nm. The local maxima are at 292 nm and 307 nm.

Calix[4]-benzimidazoyl]platinum(II) trifluoromethanesulfonate (**F**)

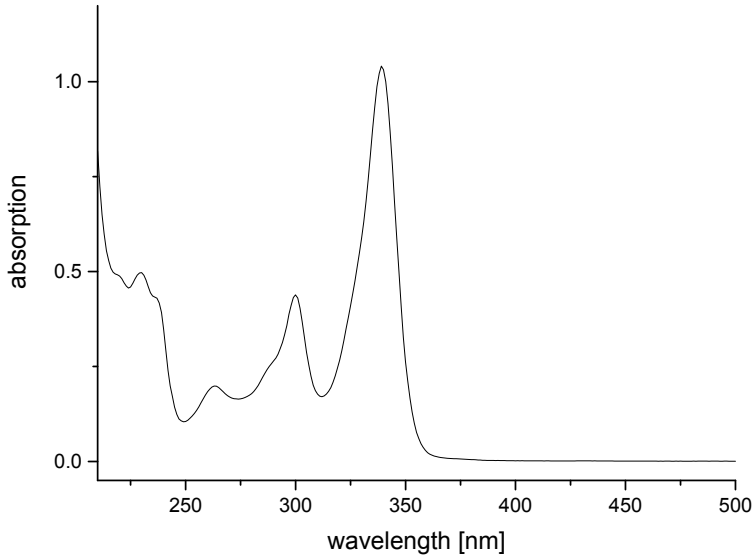

Figure 17: UV/Vis spectrum of calix[4]-benzimidazoyl]platinum(II) trifluoromethanesulfonate (**F**) in acetonitrile at 0.25 μM and a spectral range of 210 - 500 nm. The local maxima are at 230 nm, 263 nm, 300 nm and 339 nm.

Luminescence spectroscopy

Emission spectra where recorded on a Horiba Scientific FlouroMax-4P Spectrofluorometer equipped with a continuous Xe source for steady state spectra and a Xe flashlight source for the observation of phosphorescence spectra. Fluorescence spectra at room temperature were measured in quartz cuvettes (opt. path length 10 x 4 mm, excitation along the 10 mm axis). Luminescence spectra under cryogenic conditions were collected using septum sealed quartz tubes (4 mm internal diameter) placed in a small quartz Dewar vessel which was filled with liquid nitrogen for recording spectra at cryogenic temperatures (77 K). Intensities are given as counts per second (cps) for steady state measurements and as counts for time delayed measurements.

Calix[4]benzimidazolium trifluoromethansulfonate (L2)

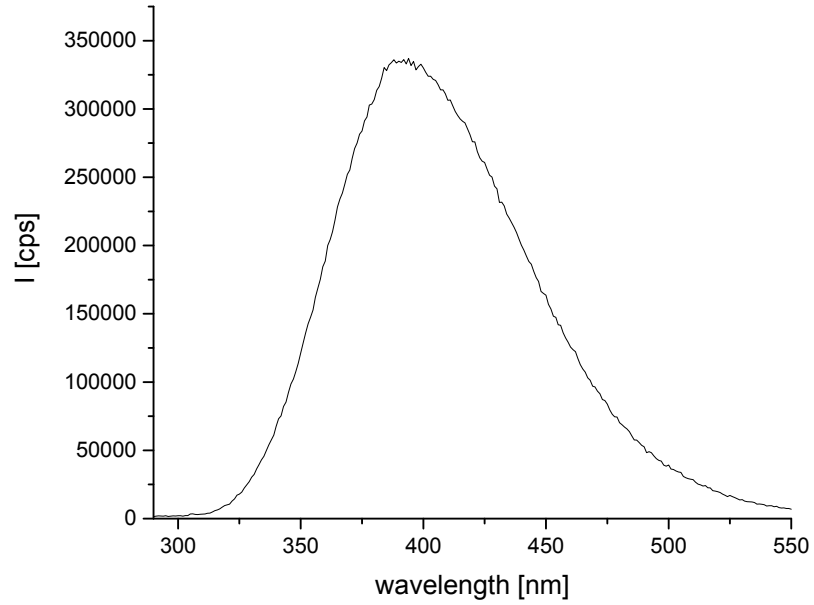

Figure 18: Fluorescence spectrum of ligand **L2** in degassed acetonitrile (c = 25 μM) at r.t., $\lambda_{exc.}$ = 280 nm.

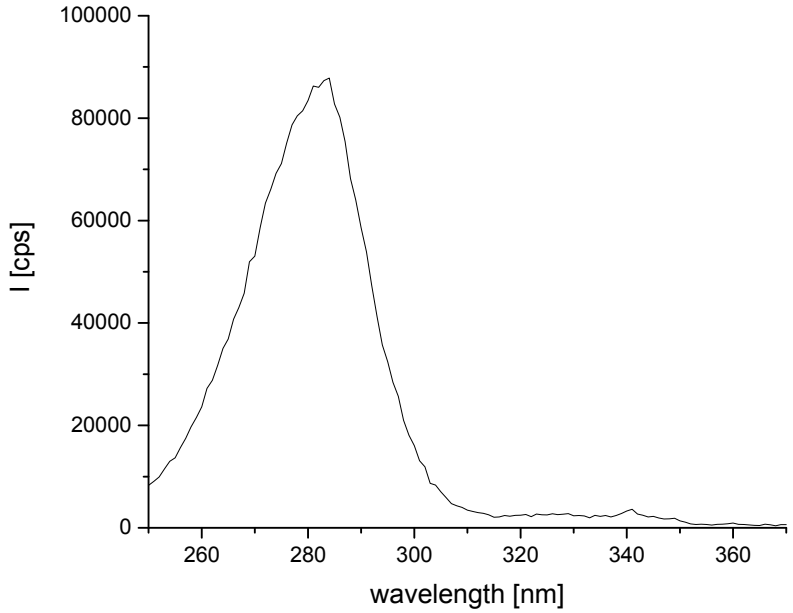

Figure 19: Excitation scan of ligand **L2** in degassed acetonitrile (c = 25 μM) at r.t..

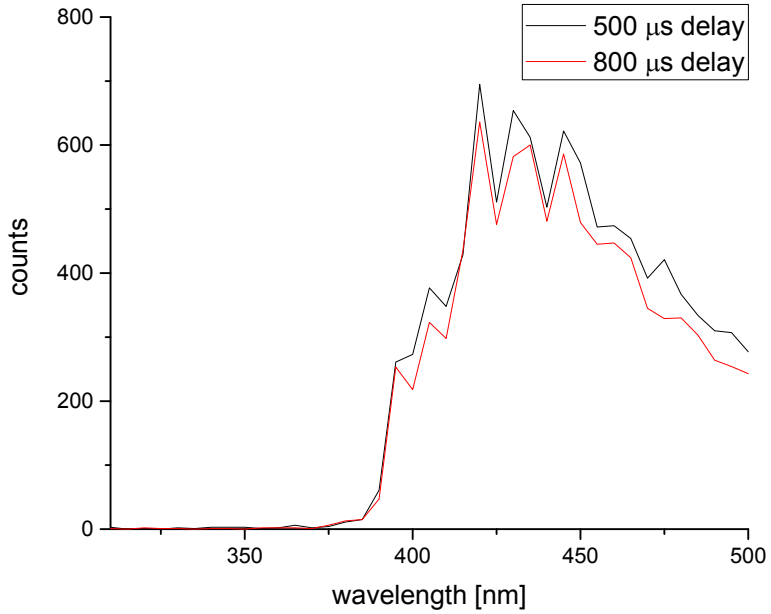

Figure 20: Time resolved spectrum of ligand **L2** in degassed acetonitrile (c = 25 μM) at 77 K after 500 and 800 μs delay, $\lambda_{exc.}$ = 275 nm.

Calix[4]-benzimidazoyl]nickel(II) trifluoromethanesulfonate (**D**)

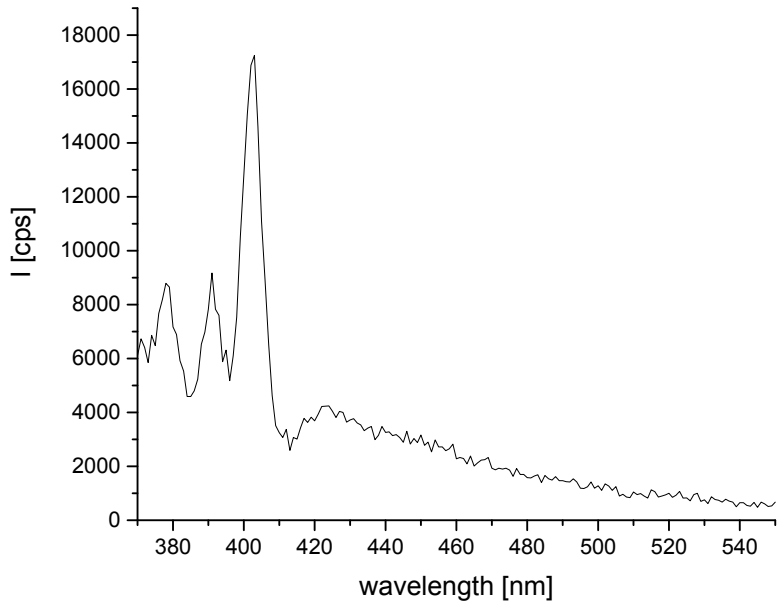

Figure 21: Luminescence spectrum of a sample of complex **D** in degassed acetonitrile (c = 25 μM) at r.t., $\lambda_{exc.}$ = 360 nm. Emission maxima have been identified as Raman signals (emission-wavelength depends on excitation wavelength).

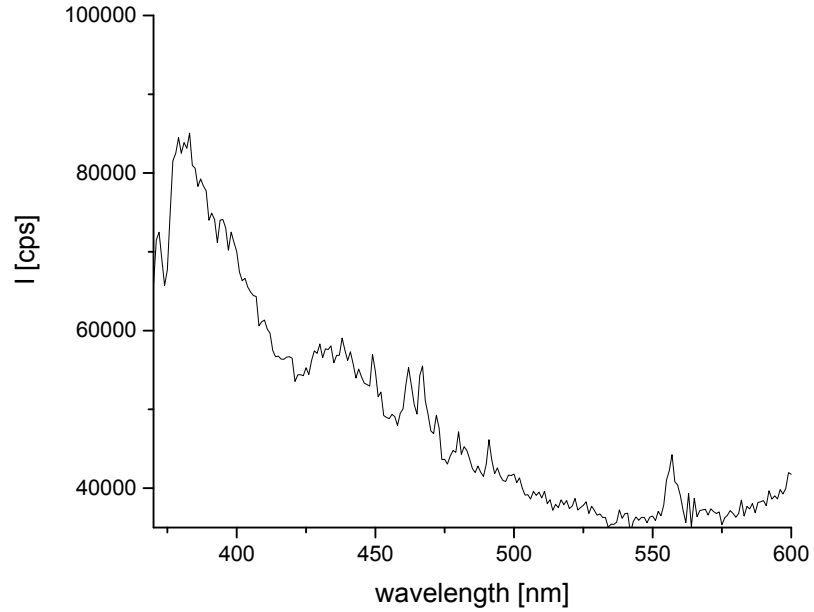

Figure 22: Luminescence spectrum of a sample of complex **D** in degassed acetonitrile (c = 25 μM) at 77 K, $\lambda_{exc.}$ = 340 nm with no signals, which can be attributed to compound **D**.

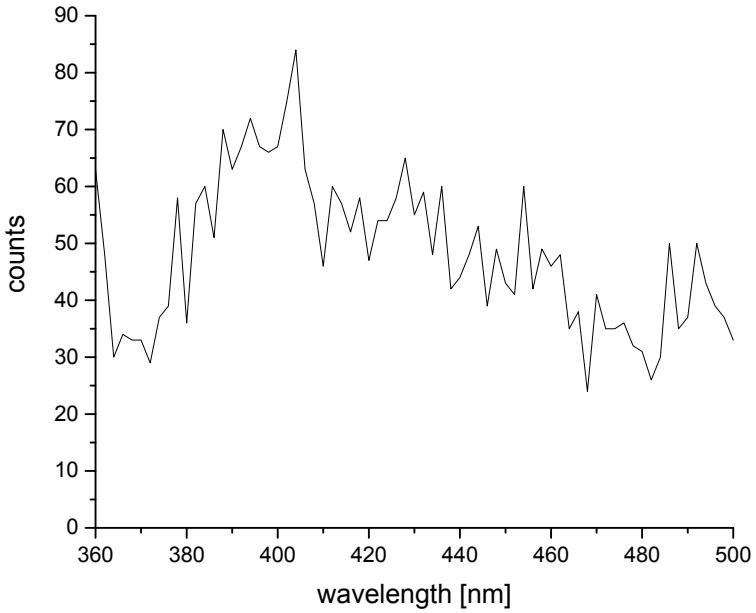

Figure 23: Time resolved luminescence spectrum of a sample of complex **D** in degassed acetonitrile (c = 25 µM) at 77 K after 100 µs delay, $\lambda_{exc.}$ = 350 nm, with no signals, which can be attributed to compound **D**.

Calix[4]-benzimidazoyl]palladium(II) trifluoromethanesulfonate (E)

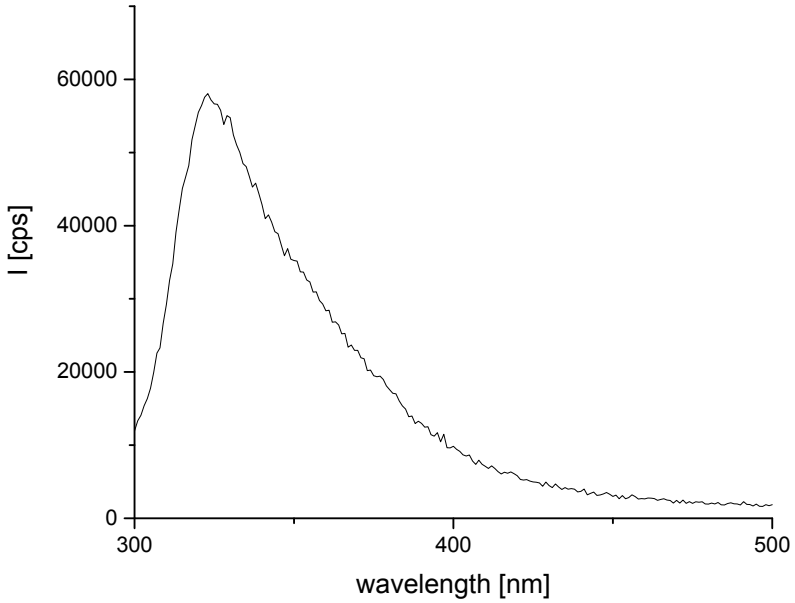

Figure 24: Fluorescence spectrum of complex **E** in degassed acetonitrile (c = 25 μM) at r.t., $\lambda_{exc.}$ = 270 nm.

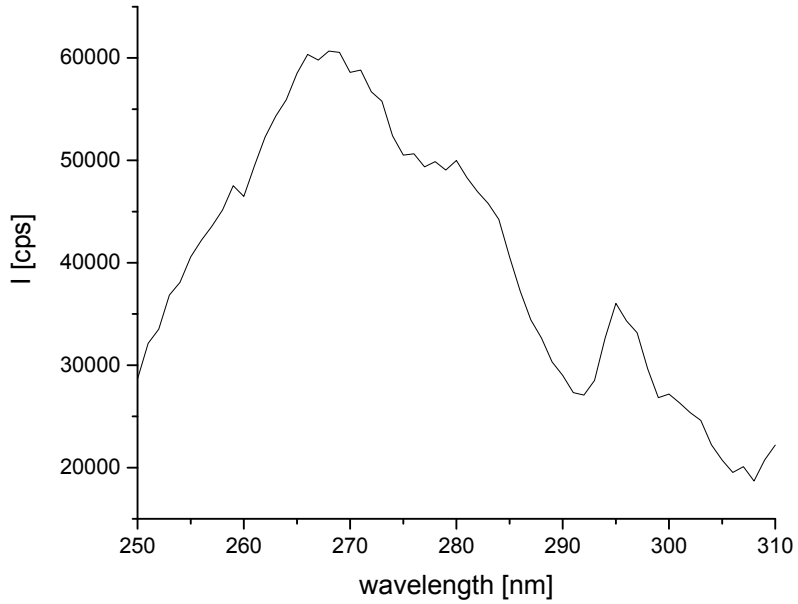

Figure 25: Excitation scan of complex **E** in degassed acetonitrile (c = 25 μM) at r.t..

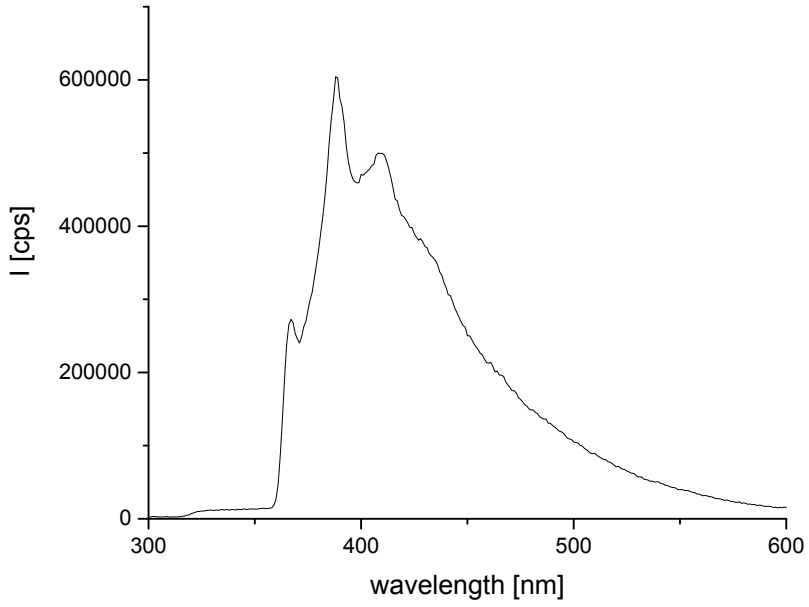

Figure 26: Luminescence spectrum of complex **E** in degassed acetonitrile (c = 25 μM) at 77 K, $\lambda_{exc.}$ = 270 nm, emission has been recorded through a WG300 filter.

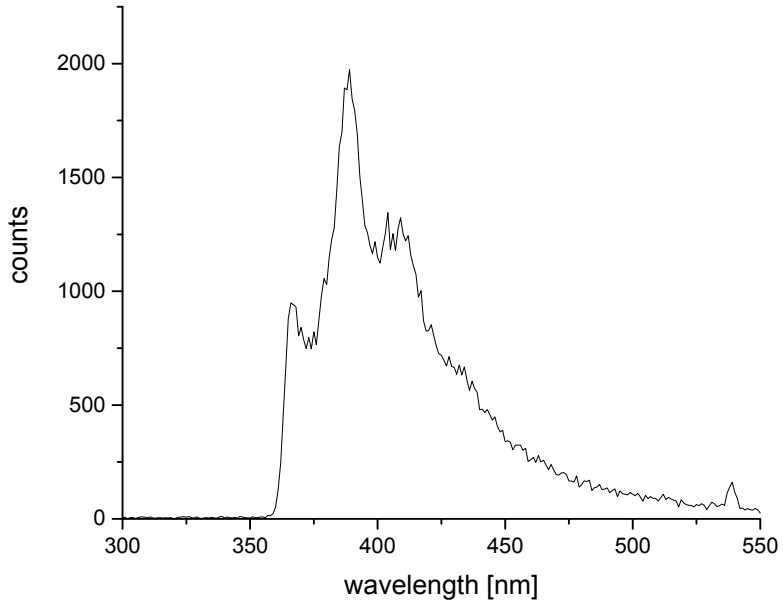

Figure 27: Time resolved luminescence spectrum of complex **E** in degassed acetonitrile (c = 25 µM) at 77 K after 1000 µs delay, $\lambda_{exc.}$ = 270 nm. The emission maxima at 367 nm adheres to a triplet energy of 326 (±1) kJ/mol.

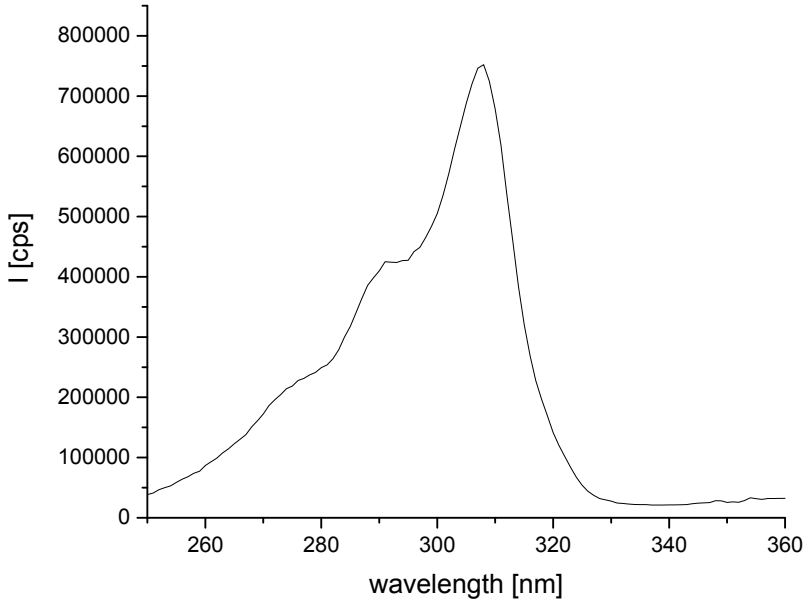

Figure 28: Excitation scan of complex **E** in degassed acetonitrile (c = 25 µM) at 77 K.

Calix[4]-benzimidazoyl]platinum(II) trifluoromethanesulfonate (F)

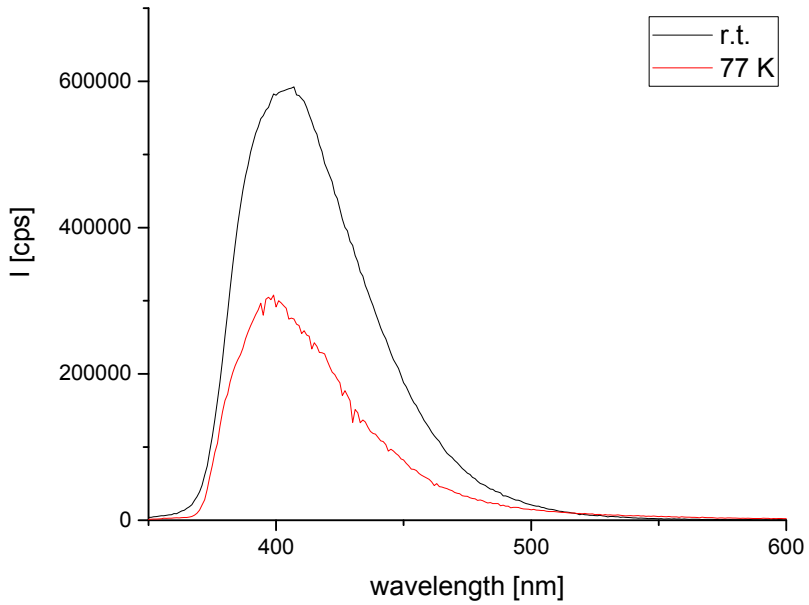

Figure 29: Fluorescence spectrum of complex **F** in degassed acetonitrile (c = 25 μM) at r.t. and 77 K, $\lambda_{exc.}$ = 330 nm.

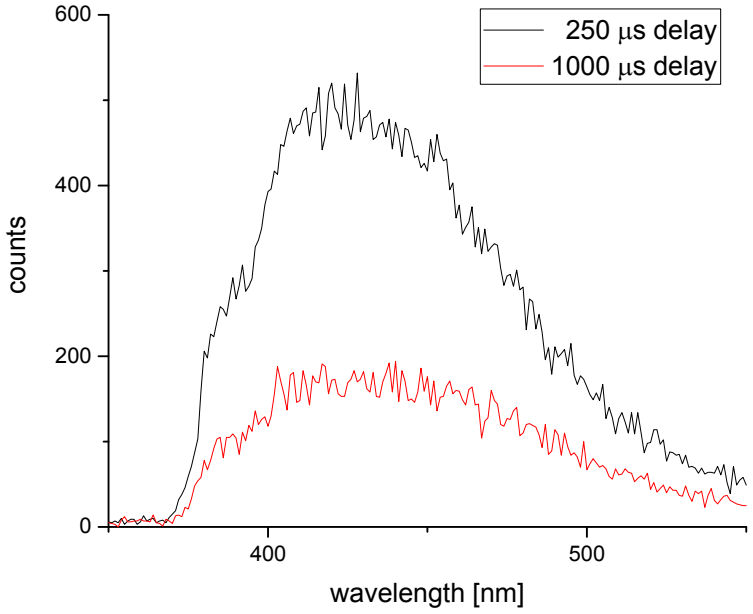

Figure 30: Time resolved spectrum of complex **F** in degassed acetonitrile (c = 25 μM) at 77 K after 250 μs delay, $\lambda_{exc.}$ = 330 nm.

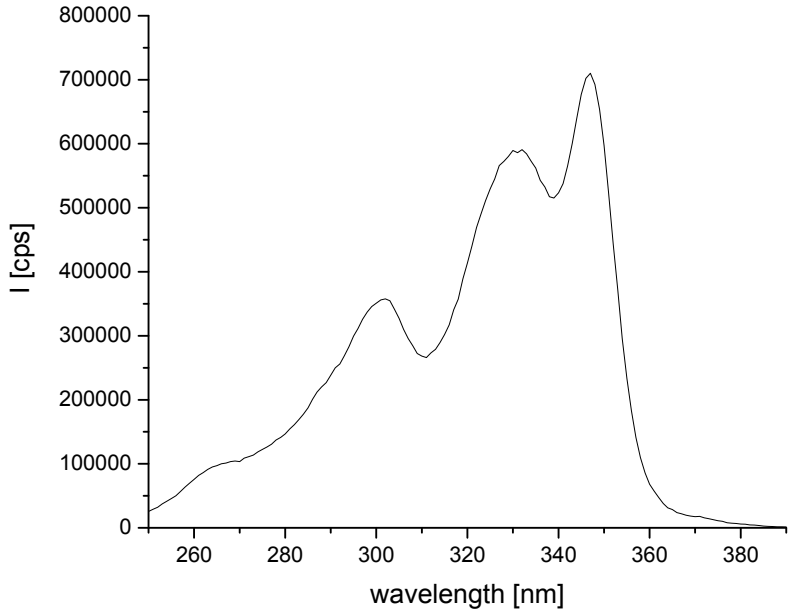

Figure 31: Excitation scan of complex **E** in degassed acetonitrile (c = 25 μM) at r.t..

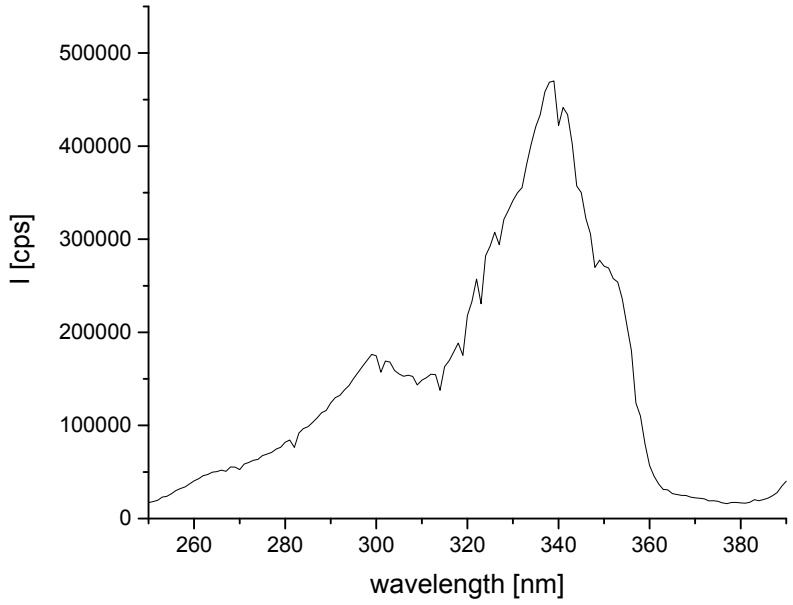

Figure 32: Excitation scan of complex **E** in degassed acetonitrile (c = 25 μM) at 77 K.

Stability studies

Stability in cell culture medium

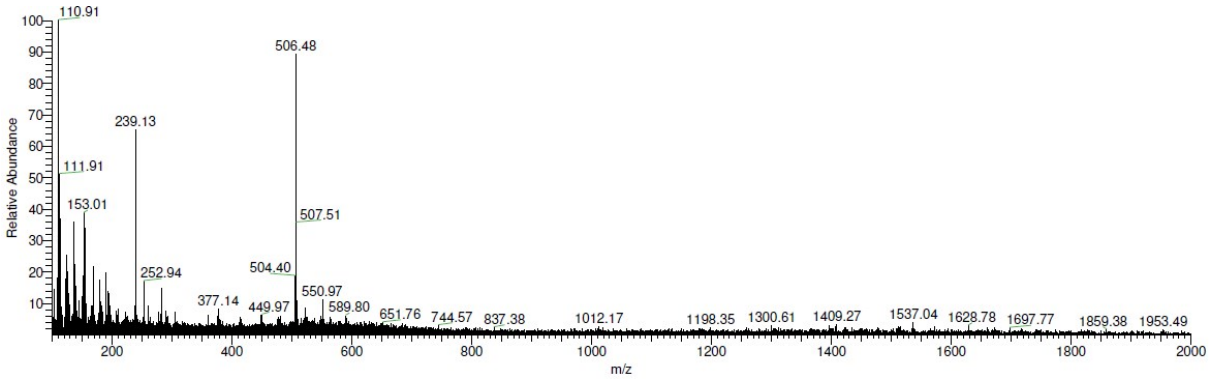

Figure 33: ESI-MS spectrum of complex **A** after incubation in RPMI1640 cell culture medium for 48 h at 37 °C.

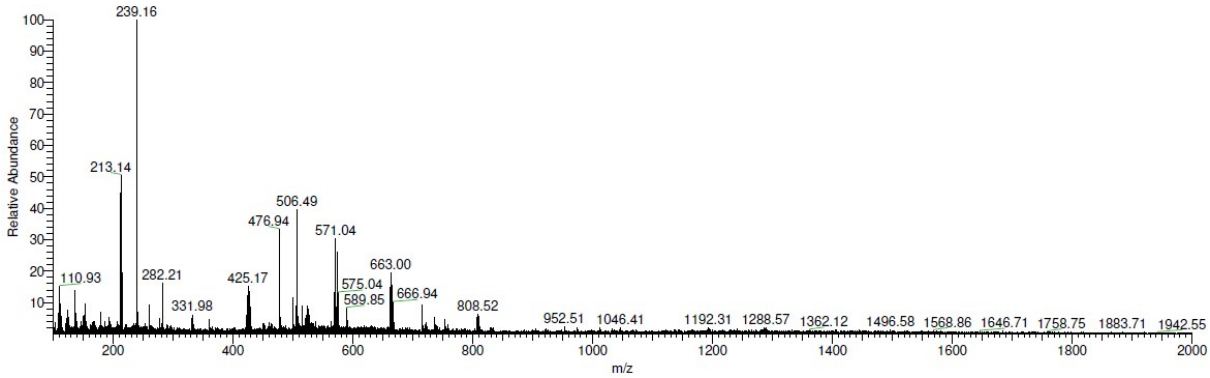

Figure 34: ESI-MS spectrum of complex **B** after incubation in RPMI1640 cell culture medium for 48 h at 37 °C.

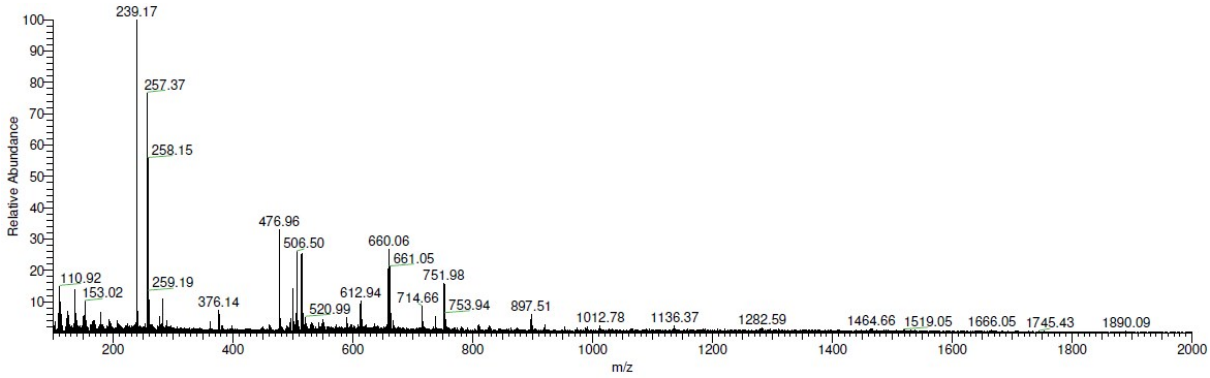

Figure 35: ESI-MS spectrum of complex **C** after incubation in RPMI1640 cell culture medium for 48 h at 37 °C.

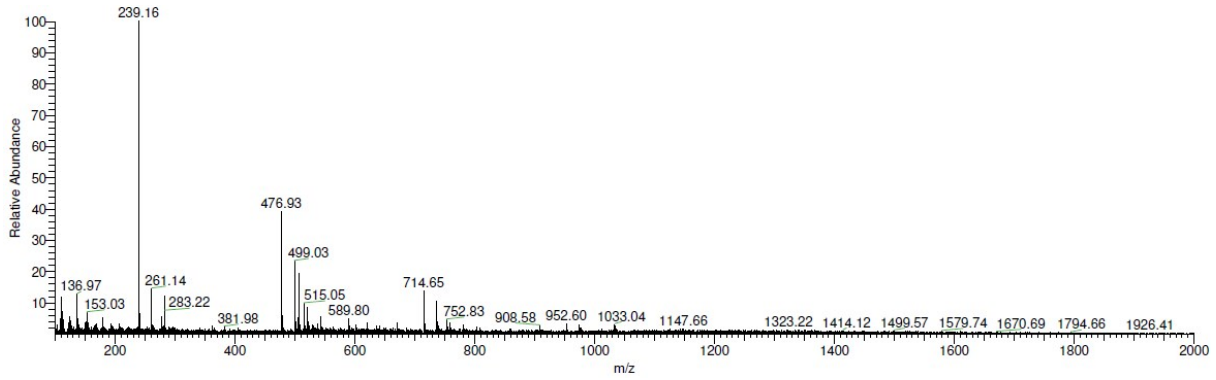

Figure 36: ESI-MS spectrum of complex **D** after incubation in RPMI1640 cell culture medium for 48 h at 37 °C.

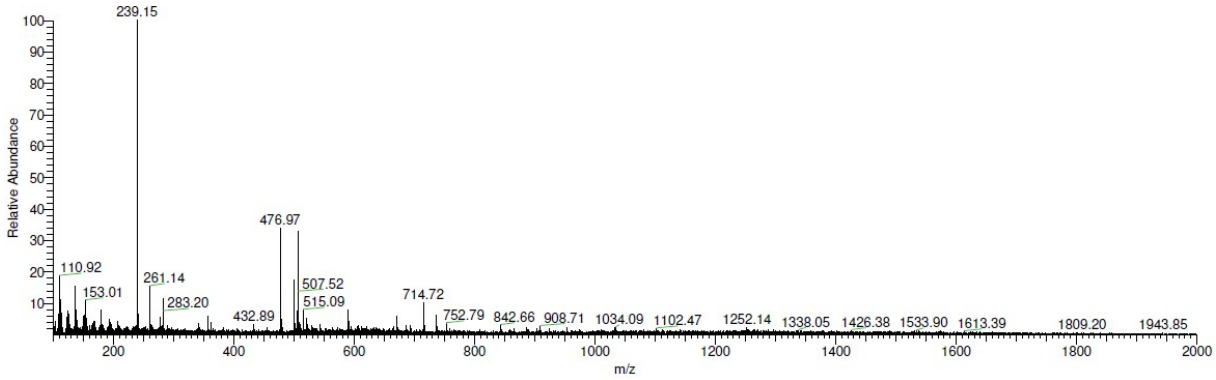

Figure 37: ESI-MS spectrum of complex **E** after incubation in RPMI1640 cell culture medium for 48 h at 37 °C.

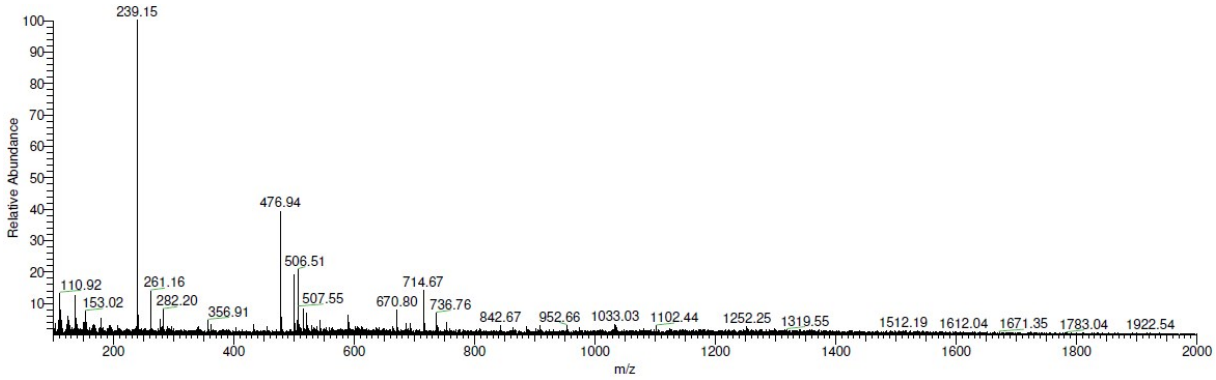

Figure 38: ESI-MS spectrum of complex **F** after incubation in RPMI1640 cell culture medium for 48 h at 37 °C.

Stability in presence of GSH

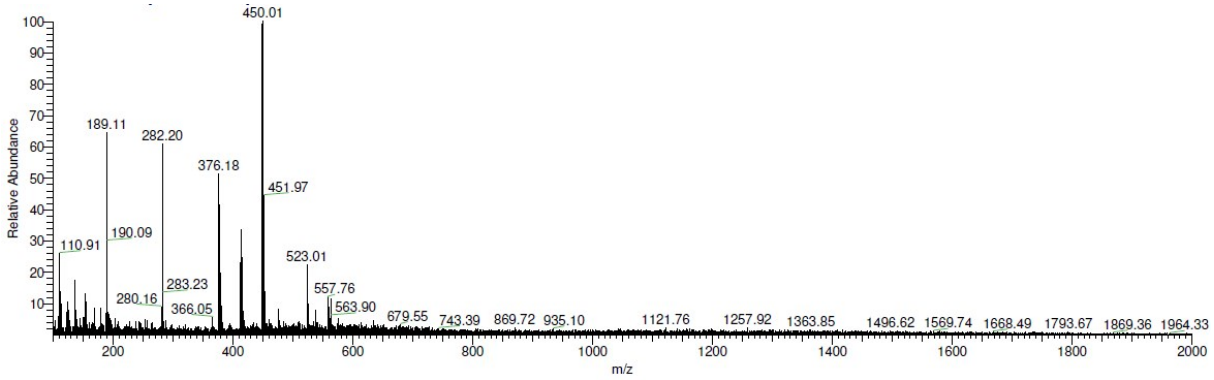

Figure 39: ESI-MS spectrum of complex **A** after 48 h of incubation in presence of GSH.

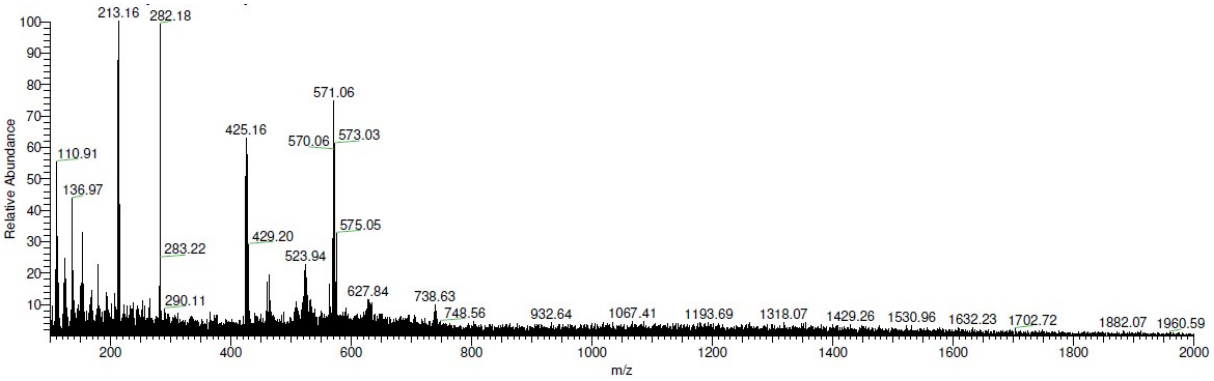

Figure 40: ESI-MS spectrum of complex **B** after 48 h of incubation in presence of GSH.

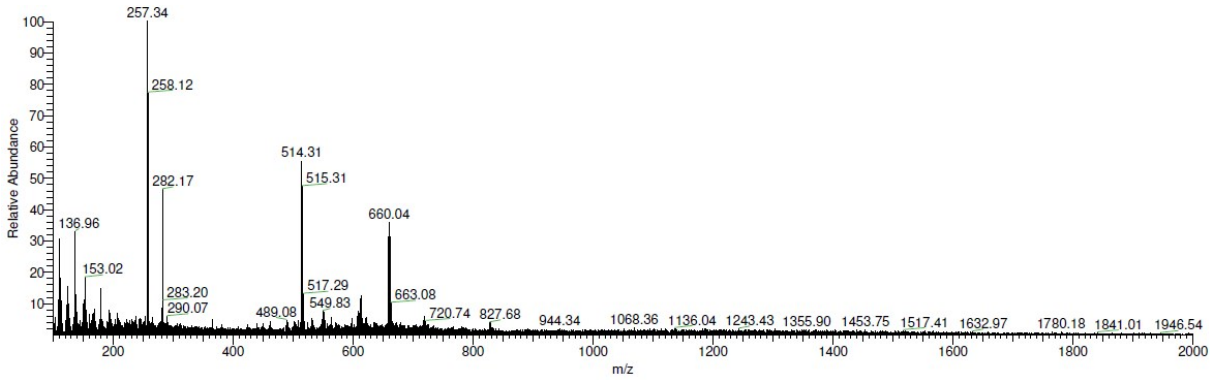

Figure 41: ESI-MS spectrum of complex **C** after 48 h of incubation in presence of GSH.

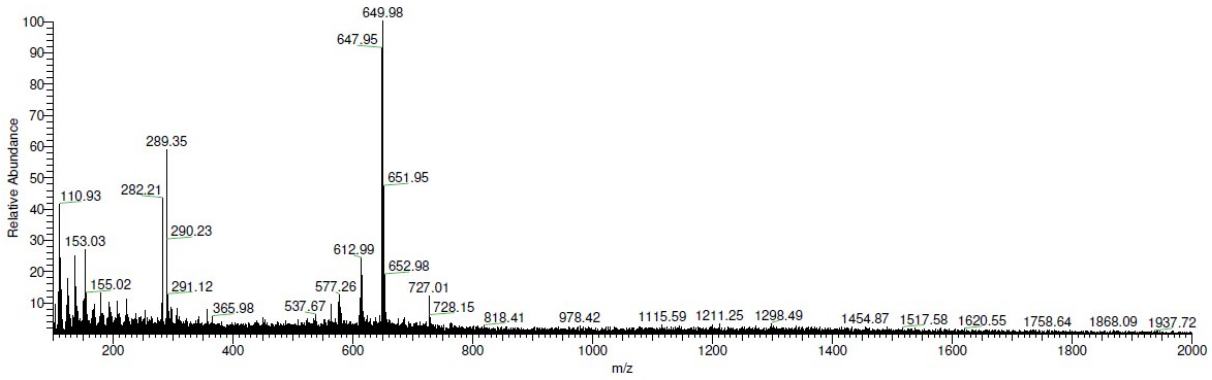

Figure 42: ESI-MS spectrum of complex **D** after 48 h of incubation in presence of GSH.

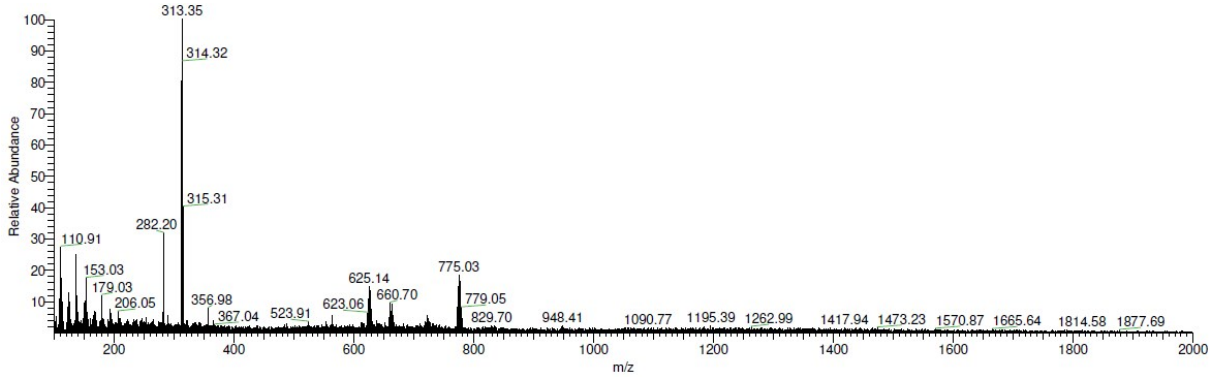

Figure 43: ESI-MS spectrum of complex **E** after 48 h of incubation in presence of GSH.

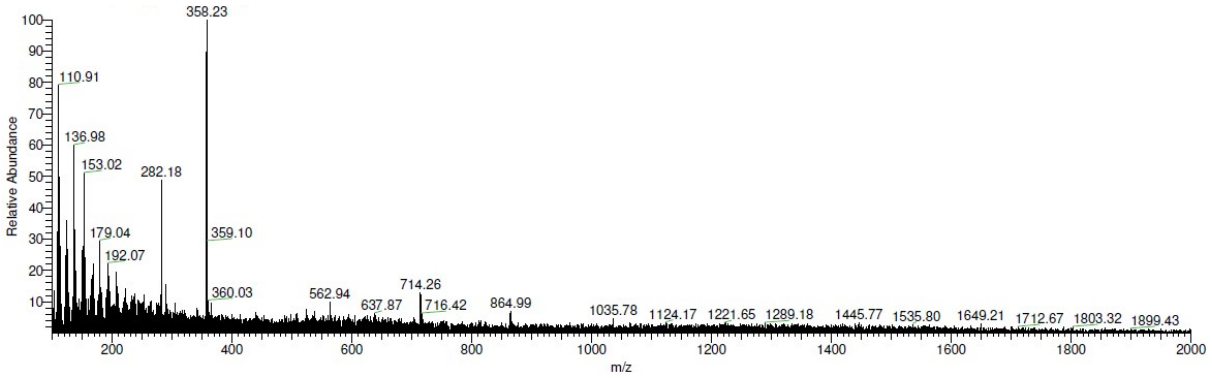

Figure 44: ESI-MS spectrum of complex **F** after 48 h of incubation in presence of GSH.

MTT assays

Table 2: IC_{50} values [µM] determined for complexes **A**-**F**, ligands **L1** and **L2** as well as cisplatin in MTT assays in cervix cancer (HeLa), breast cancer (MCF-7) and cisplatin-resistant ovarian cancer cells using an incubation period of 48 h.

Compound	HeLa	MCF-7	A2780cisR
A	63.6 ± 23	70.3 ± 11	84.5 ± 12
B	2.8 ± 1.3	1.3 ± 0.1	1.9 ± 1.0
C	2.9 ± 1.3	1.4 ± 0.1	1.7 ± 0.3
D	n.a.	n.a.	n.a.
E	0.4 ± 0.2	n.a.	0.1 ± 0.01
F	0.5 ± 0.1	n.a.	0.2 ± 0.2
L1	72.2 ± 19(24)	85.5 ± 3.3(24)	88.8 ± 9(24)
L2	n.d.	n.d.	n.d.
cisplatin	2.8 ± 0.5(24)	4.7 ± 0.9(24)	10.9 ± 1.7(24)

n.a. = not active (IC_{50} > 100 µM)

n.d. = not determined; due to water sensitivity

HeLa cells

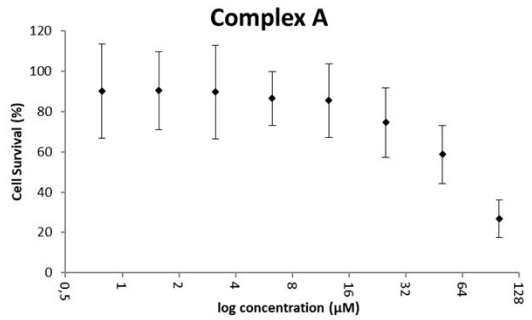

Figure 45: Cell survival [%] of HeLa cells determined *via* MTT assays. Cells treated with varying concentrations of complex **A** for 48 h. The standard deviation is calculated using three independent measurements.

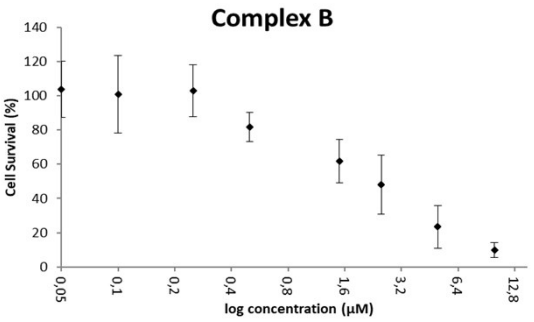

Figure 46: Cell survival [%] of HeLa cells determined *via* MTT assays. Cells treated with varying concentrations of complex **B** for 48 h. The standard deviation is calculated using three independent measurements.

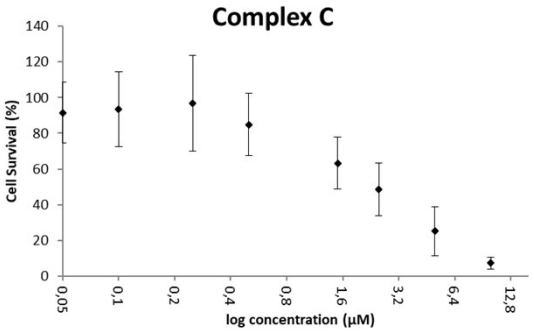

Figure 47: Cell survival [%] of HeLa cells determined *via* MTT assays. Cells treated with varying concentrations of complex **C** for 48 h. The standard deviation is calculated using three independent measurements.

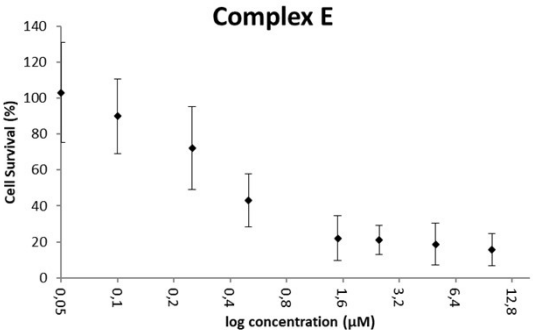

Figure 48: Cell survival [%] of HeLa cells determined *via* MTT assays. Cells treated with varying concentrations of complex **E** for 48 h. The standard deviation is calculated using three independent measurements.

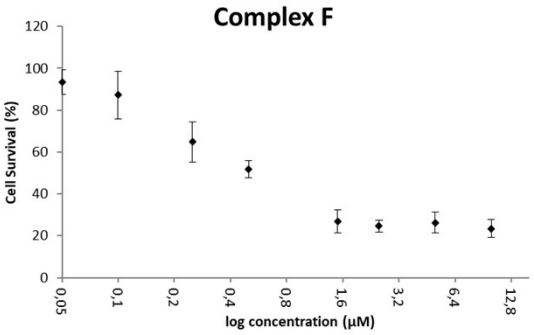

Figure 49: Cell survival [%] of HeLa cells determined *via* MTT assays. Cells treated with varying concentrations of complex **F** for 48 h. The standard deviation is calculated using three independent measurements.

MCF-7 cells

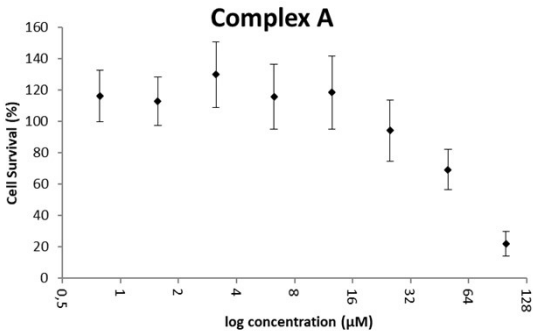

Figure 50: Cell survival [%] of MCF-7 cells determined *via* MTT assays. Cells treated with varying concentrations of complex **A** for 48 h. The standard deviation is calculated using three independent measurements.

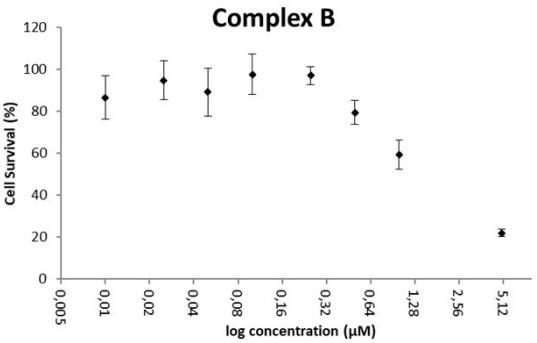

Figure 51: Cell survival [%] of MCF-7 cells determined *via* MTT assays. Cells treated with varying concentrations of complex **B** for 48 h. The standard deviation is calculated using three independent measurements.

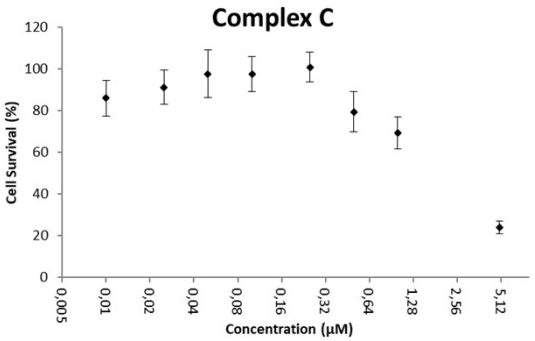

Figure 52: Cell survival [%] of MCF-7 cells determined *via* MTT assays. Cells treated with varying concentrations of complex **C** for 48 h. The standard deviation is calculated using three independent measurements.

A2780cisR cells

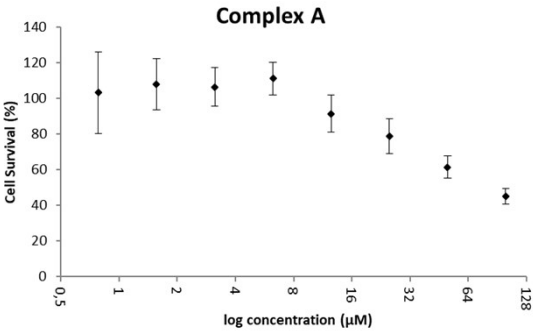

Figure 53: Cell survival [%] of A2780cisR cells determined *via* MTT assays. Cells treated with varying concentrations of complex **A** for 48 h. The standard deviation is calculated using three independent measurements.

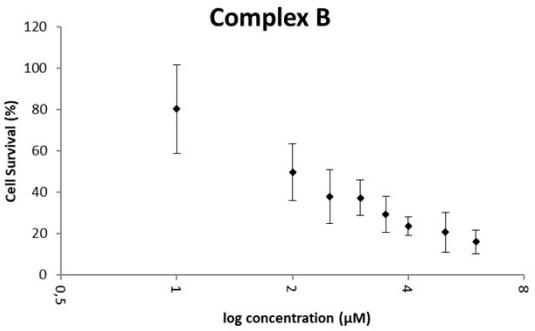

Figure 54: Cell survival [%] of A2780cisR cells determined *via* MTT assays. Cells treated with varying concentrations of complex **B** for 48 h. The standard deviation is calculated using three independent measurements.

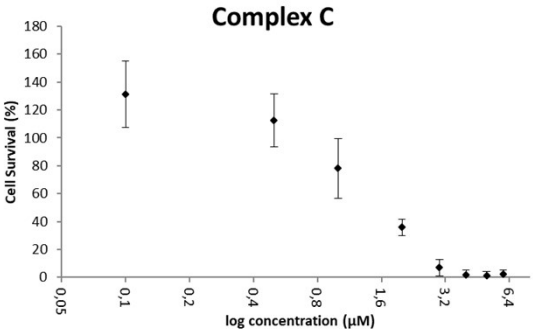

Figure 55: Cell survival [%] of A2780cisR cells determined *via* MTT assays. Cells treated with varying concentrations of complex **C** for 48 h. The standard deviation is calculated using three independent measurements.

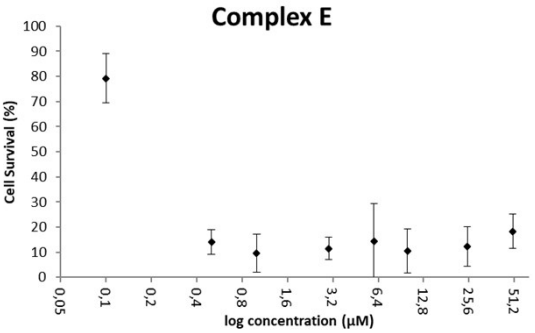

Figure 56: Cell survival [%] of A2780cisR cells determined *via* MTT assays. Cells treated with varying concentrations of complex **E** for 48 h. The standard deviation is calculated using three independent measurements.

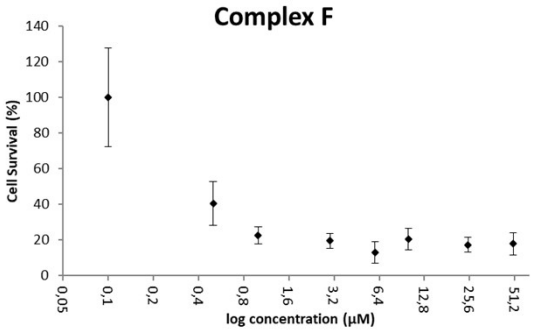

Figure 57: Cell survival [%] of A2780cisR cells determined *via* MTT assays. Cells treated with varying concentrations of complex **F** for 48 h. The standard deviation is calculated using three independent measurements.